https://doi.org/10.5194/egusphere-2026-1865
Preprint. Discussion started: 21 May 2026

First deployment of active AirCore in a volcanic plume at Mount Etna

Johannes Degen[1], Nicole Bobrowski[2, 3], Mélisende M. Bossard[3, 4], Lucie Boucher[3, 5], Huilin Chen[6, 7], Andreas Engel[1], Bastien H. Geil[8], Giovanni B. Giuffrida[3], Steven van Heuven[6], Thorsten Hoffmann[8], Niklas Karbach[8], Gianluigi Ortenzi[3], and Tanja J. Schuck[1]

[1]Institute for Atmospheric and Environmental Sciences, Goethe University Frankfurt, Frankfurt, Germany
[2]Institute of Environmental Physics, Heidelberg University, Heidelberg, Germany
[3]Istituto Nazionale di Geofisica e Vulcanologia, Osservatorio Etneo, Catania, Italy
[4]École et Observatoire des Sciences de la Terre, Strasbourg University, Strasbourg, France
[5]École Normale Supérieure de Paris, Paris Sciences et Lettres University, Paris, France
[6]Centre for Isotope Research, University of Groningen, Groningen, the Netherlands
[7]School of Atmospheric Sciences, Nanjing University, Nanjing, China
[8]Department of Chemistry, Johannes Gutenberg-Universität Mainz, Mainz, Germany

Correspondence: Johannes Degen (degen@iau.uni-frankfurt.de)

Abstract. Uncrewed Aerial Systems (UAS) are by now well established platforms for observations in volcanic plumes which are a challenging environment. Options for trace gas observations inside volcanic plumes still remain limited because sophisticated measurement techniques for high-precision observations of trace gases often require instrumentation that cannot be used on board UAS due to high weight and power consumption. UAS-borne sampling of air followed by post-flight analysis can extend the number of observable trace gases as well as the measurement quality. Originally developed for stratospheric observations, AirCore sampling with long coiled tubes has proven to be a light-weight sampling technique to probe parts of the atmosphere that are otherwise difficult to access. Trace gas analysis of sampled air is done post-flight, most commonly with fast high-precision optical methods with continuous flow analysers, delivering high-quality and high-resolution trace gas mole fractions. While balloon-borne AirCore setups perform passive sampling making use of natural pressure differences, we used a UAS-deployable small active AirCore setup collecting air with a pump. In July 2024, this setup was deployed on a UAS alongside electrochemical and optical gas sensors to probe the volcanic plumes of Mount Etna (Sicily, Italy), which was particularly active at the time. This was to our knowledge the first time that the AirCore sampling technique was used inside volcanic plumes. The air sample was successfully analysed with cavity-ring down spectroscopy for carbon monoxide (CO), carbon dioxide (CO_2) and methane (CH_4). While CO_2 and often also CO mole fractions were markedly enhanced in the plume, no significant change of CH_4 was observed. The ratio of CO and CO_2 mole fraction enhancements was found to be rather low which might point at fast oxidation processes.

https://doi.org/10.5194/egusphere-2026-1865
Preprint. Discussion started: 21 May 2026

1 Introduction

Volcanoes are an important channel for transporting material from the Earth's interior to the planet's surface. Volcanic emissions can alter Earth's atmosphere by gradually changing its composition or its redox state over long periods of time (Moussallam et al., 2019), and in the short term when enormous quantities are released during highly explosive eruptions (Timmreck, 2012). Volcanic gaseous emissions therefore present an interconnection between the deep and shallow carbon cycles on Earth (Burton et al., 2013; Foley and Fischer, 2017; Plank and Manning, 2019). Carbon dioxide (CO_2) is one of the major constituents of volcanic gaseous emissions with total annual emissions from non-eruptive degassing estimated $51.3 \pm 5.7\,\mathrm{Tg\,CO_2}$ for the period 2005–2015 (Fischer et al., 2019). While this number may appear small compared to today's anthropogenic emissions from fossil fuel burning estimated at $36800 \pm 1800\,\mathrm{Tg\,CO_2\,yr^{-1}}$ in 2023 (Friedlingstein et al., 2025), quantifying volcanic emissions is nevertheless needed for a full understanding of the global carbon budget and in general Earth's history. Mount Etna (Sicily, Italy, 37 °N 45'4"N, 14 °E 59'45") is one of the most active volcanoes on Earth, emitting large amounts of CO_2 (~10 % of the global volcanic CO_2 emissions; Burton et al., 2013) with a high temporal variability (Aiuppa et al., 2006; La Spina et al., 2010; Pering et al., 2014).

Beside the impact of volcanic gases on atmosphere, hydrosphere and biosphere, their chemical composition and amount and especially their changes over time, can also provide information on the fundamental physical and chemical processes underneath the surface. Measurements of chemical composition of volcanic plumes are a useful method of volcano monitoring (Symonds et al., 1994; Edmonds, 2008). It has been discussed whether a connection can be established between the redox state of volcanic gases and their magmatic source, i. e. whether the redox signature of the gas-releasing magma (f_{O_2}) can be deduced from the measurements of corresponding gaseous redox pairs, for example CO_2/CO, or SO_2/H_2S (Burgisser and Scaillet, 2007; Oppenheimer et al., 2018; Moussallam et al., 2019; Moretti and Stefánsson, 2020; Kuhn et al., 2022). Magma temperature and redox state correlate to some degree with the ratio of SO_2 to H_2S and the amounts of gas species like H_2, CO, or OCS. Therefore, quantification of the composition of the magmatic gases might allow conclusions about the redox state of the magma as well as the temperature at which the gas was last in equilibrium with the surrounding magma. As possible overlying influencing factors of the gas redox state, gas-rock and gas-liquid interactions are discussed in the literature, particularly for the study of colder fumarole emissions (Giggenbach, 1996). To further support and prove novel model studies, comparisons to measurement data are essential, but only very limited data sets of redox pairs in volcanic plumes are available. Only spatially resolved measurements can take into account plume age which is a relevant parameter as the gas composition in the plume might deviate from the initial volcanic gas composition (Kuhn et al., 2022).

With high mole fractions, high temperatures and a high load of particles, volcanic plumes are a harsh, acidic environment where in-situ operation of instruments is challenging. Therefore, remote-sensing spectrometry techniques such as differential optical absorption spectroscopy and Fourier-transform infrared spectroscopy, provide a number of advantages (Oppenheimer and McGonigle, 2009; Platt et al., 2018) and are more and more often used to probe the chemical composition of volcanic plumes. However, many of the redox pairs can often not be determined under quiescent degassing conditions. Due to the high and variable background mole fraction of CO_2 and H_2O remote sensing usually does not allow the quantification of those

https://doi.org/10.5194/egusphere-2026-1865
Preprint. Discussion started: 21 May 2026

components in volcanic plumes with few exceptions (Goff et al., 2001; Butz et al., 2017). Also CO and H_2S are only detectable under favourable conditions, because the atmospheric background of CO with about 100 ppb is relatively high in comparison to the mole fraction increase in a volcanic plume and H_2S has only weak absorption bands.

Aged volcanic plumes can be probed with aircraft equipped with state of the art instrumentation for trace gases (Rose et al., 2006; Oppenheimer et al., 2010; Baker et al., 2011; Heue et al., 2011; Rauthe-Schöch et al., 2012; Voigt et al., 2014) or aerosols (Martinsson et al., 2009, 2017). However, aircraft measurements are very cost intensive and need a very long planning time in advance, therefore most available measurements were performed unintentionally when crossing volcanic plumes by chance.

Direct measurements with instrumentation carried by Uncrewed Aerial Systems (UAS) can be a valuable alternative. Nowadays, gases inside volcanic plumes are commonly measured with in-situ multi-gas analyser packages deploying electrochemical or optical sensors carried by UAS (James et al., 2020; Liu et al., 2019; Karbach et al., 2022). The main advantage of such sensor systems is their low weight and low power consumption. But this comes at the price of accuracy, specificity and sensitivity as well as often limited lifetime of the sensors. Many sensors show only a ppm resolution and have to be corrected for cross interferences with other gases, temperature, pressure and humidity dependencies as well as for long response times (Roberts et al., 2014, 2019).

For atmospheric observations of CO and CO_2, state of the art instrumentation are fast optical continuous-flow analysers which are usually deployed for direct in-situ measurements (Crosson, 2008; Karion et al., 2013), but are also frequently used for post-flight measurements of air sampled with the AirCore technique. AirCore sampling is a method that was developed to access remote parts of the atmosphere, namely for sampling the stratosphere at altitudes inaccessible for aircraft (Tans, 2009; Karion et al., 2010). In the original setup, AirCore is a passive sampling technique that relies on the vertical pressure gradient in the atmosphere. The devices with typical weights around 3 kg are launched with small weather balloons up to maximum altitudes around 30 km. They consist of long thin-walled stainless steel tubes that are open on one end and closed at the other. Prior to launch, the tube is filled with a so-called fill gas (FG) that escapes during ascent with decreasing ambient pressure. At altitude, the balloon bursts and the payload is descending, decelerated by a parachute. With now increasing pressure, the sample is collected passively into the evacuated tube, finally representing a vertical profile of the atmosphere. Due to the small tube diameter, diffusion is slow and spatial information, in this case altitude, is preserved for some time. Upon recovery of the payload, the sample is brought to a laboratory. Most commonly it is analysed with continuous-flow cavity-ringdown spectroscopy instruments, but also subsampling the AirCore sample has been done to apply other analysis techniques (e.g. Laube et al., 2025). Investigations on the influence of AirCore coil configurations on resolution (Membrive et al., 2017) and filling dynamics (Tans, 2022) have contributed to making this technology interesting for other applications.

Andersen et al. (2018) have developed this method further towards active sampling with a pump. Thus, the sample can be collected irrespectively of pressure gradients, however, at the expense of adding complexity to the setup. Using UAS instead of balloons as platforms, spatially resolved sampling of air on flexible trajectories for subsequent post-flight high-precision analysis becomes possible. This was successfully demonstrated investigating the diurnal cycle of the planetary boundary layer and comparing the results from AirCore sampling to fixed-site observations with a series of five flights (Andersen et al., 2018).

https://doi.org/10.5194/egusphere-2026-1865
Preprint. Discussion started: 21 May 2026

In July 2024, an active AirCore setup similar to the one described by Andersen et al. (2018) was deployed at Mt. Etna on a UAS in combination with Multi-component Gas Analyser System (Multi-GAS) packages to probe the volcano's degassing of CO, CO_2 and CH_4. To our knowledge, this was the first time that air sampling with an AirCore was performed inside a volcanic plume.

2 Experimental methods

2.1 UAS and site description

For our investigations of the volcanic plume composition at Mt. Etna, Italy, we deployed a DJI Matrice 350® multirotor UAS equipped with various scientific instruments. The weight of the drone itself including batteries was approximately 6.5 kg, allowing a payload of up to 2.5 kg and a maximum flight duration of up to 30 min. To reduce the risk of losing the UAS in a harsh and inaccessible terrain, flight duration was limited to 20 min for the plume investigations. The payload varied between flights, in addition to the active AirCore three different sensor packages were included in changing configurations. During the campaign from 2. to 11. July 2024, 20 flights were performed in total, with the active AirCore on board of the UAS during eleven flights (cf. Table 1).

All of these eleven flights were directed to the summit region of Mt. Etna, starting at 37 °N 44'9.24"N, 15 °E 0'0.36" and at an altitude of 2850 m amsl, from the edge of the inactive Barbagallo Crater. During the campaign, volcanic gas emissions were mainly observed from the Voragine crater (VOR), which even generated lava fountains during this period, and from the South-East crater (SEC) with possibly two vents. Degassing was also observed from the Bocca Nuova crater but its plume cannot be distinguished from the one from VOR. Figure 1 summarizes the trajectories of all flights that had the active AirCore as part of the payload, each targeting the summit craters which were located approximately 400–600 m above and roughly 1–2 km away from the launch area. During flights, maximum altitudes of 3420 m amsl were reached and more than 30 volcanic plume encounters, i. e. flying into and out of a single plume, could be performed (cf. Section 2.6).

2.2 Active AirCore setup

AirCore samplers are devices designed for spatially resolved air sampling, followed by offline analysis. The active AirCore approach extends the technique originally developed for passive balloon-borne stratospheric sampling that relies on the vertical pressure gradient in the atmosphere (Tans, 2009; Karion et al., 2010). While retaining a similar tube geometry, it uses pump-driven sampling, enabling deployment on UAS (Andersen et al., 2018) or other moving platforms where no natural pressure gradient is available for sampling (Tong et al., 2023; Westra et al., 2024). This allows for spatially resolved sampling along flexible trajectories.

Figure 2c shows a schematic of the sampling setup used here, which is based on the design described by Andersen et al. (2018). The AirCore consists of a ~75 m long stainless steel tube with an inner diameter of 2.9 mm and a total volume of ~500 cm^3 coated with Silconert® to passivate its inner surface. During sampling, air is drawn into the tube with a micropump

https://doi.org/10.5194/egusphere-2026-1865
Preprint. Discussion started: 21 May 2026

Table 1. Overview of individual flights with active AirCore samples in volcanic plumes. Note that during Flights F01 and F02 the Multi-GAS sensor system was not operated, and during flights F05 and F07 the AirCore sampling was interrupted because of power cuts.

flight code	date	sampling interval [UTC]	storage time [min]
F01 [a]	5. July 2024	09:59–10:12	47
F02 [a]	5. July 2024	09:24–09:46	63
F04	5. July 2024	12:52–13:03	71
F05 [b]	6. July 2024	09:52–10:04	45
F07 [b]	6. July 2024	12:37–12:51	61
F09	8. July 2024	08:08–08:25	45
F10	8. July 2024	10:37–10:54	58
F11	8. July 2024	12:14–13:29	71
F12	9. July 2024	08:42–08:59	50
F17 [c]	10. July 2024	11:52–12:07	113
F20 [c]	11. July 2024	10:17–10:37	107

[a] No data from CO_2 and SO_2 sensors.
[b] Interruption of AirCore pump flow in flight.
[c] AirCore analysed at Milo village.

(KNF NMP015). A short polyvinylchloride tube (15 cm, 1/4") is attached in front of the inlet and is loosely filled with glass wool and magnesium perchlorate $Mg(ClO_4)_2$ to act as a filter/protection for the AirCore and as a dryer. An orifice (50 ± 10 µm diameter, Lenox laser Inc.) is placed between the pump and the end of the coil to ensure a critical flow of 22 sccm (standard cubic centimetres per minute) through the AirCore. Moreover, there is a u-shaped stainless steel adapter piece to enable easy connection of the sampler to the analyser system as shown in Fig. 2d.

The control unit is a custom printed circuit board consisting of a LoRa RF95 Radio chip for transmitting data, monitoring the filling amount and remotely controlling the pump, a battery pack for power supply (2 x 18650 Li-Ion 7.4 V battery) and a data logger. This data logger is built from an Adafruit "Featherwing" system based on an ESP32 Feather Board including a RTC + SD Add-on, an OLED display, an Ultimate GPS module and several temperature (PT100, Innovative Sensor Technology) and pressure sensors (AMSYS AMS 5915; one barometric, one absolute and two differential pressure sensors). Moreover, a CO_2 sensor (Senseair K30 FR) was added for in-flight online plume detection. More technical details of the components are listed in supplementary Table 1. The whole setup got attached to the UAS using a mounting frame designed to match the drone's geometry with cable ties as shown in Fig. 2b. The total weight of the payload was approximately 1.2 kg.

Prior to flight, the AirCore was leak-checked and flushed with a well-characterised gas mixture, the fill gas (FG). Upon completion of the checks, the AirCore tube remained filled with the FG at the respective ambient pressure. During transport, the inlet was closed with a stainless-steel cap, that was removed prior to take-off and attached again immediately after landing. To protect the materials in the acidic environment of the volcanic plumes, the AirCore was wrapped in plastic foil for each

https://doi.org/10.5194/egusphere-2026-1865
Preprint. Discussion started: 21 May 2026

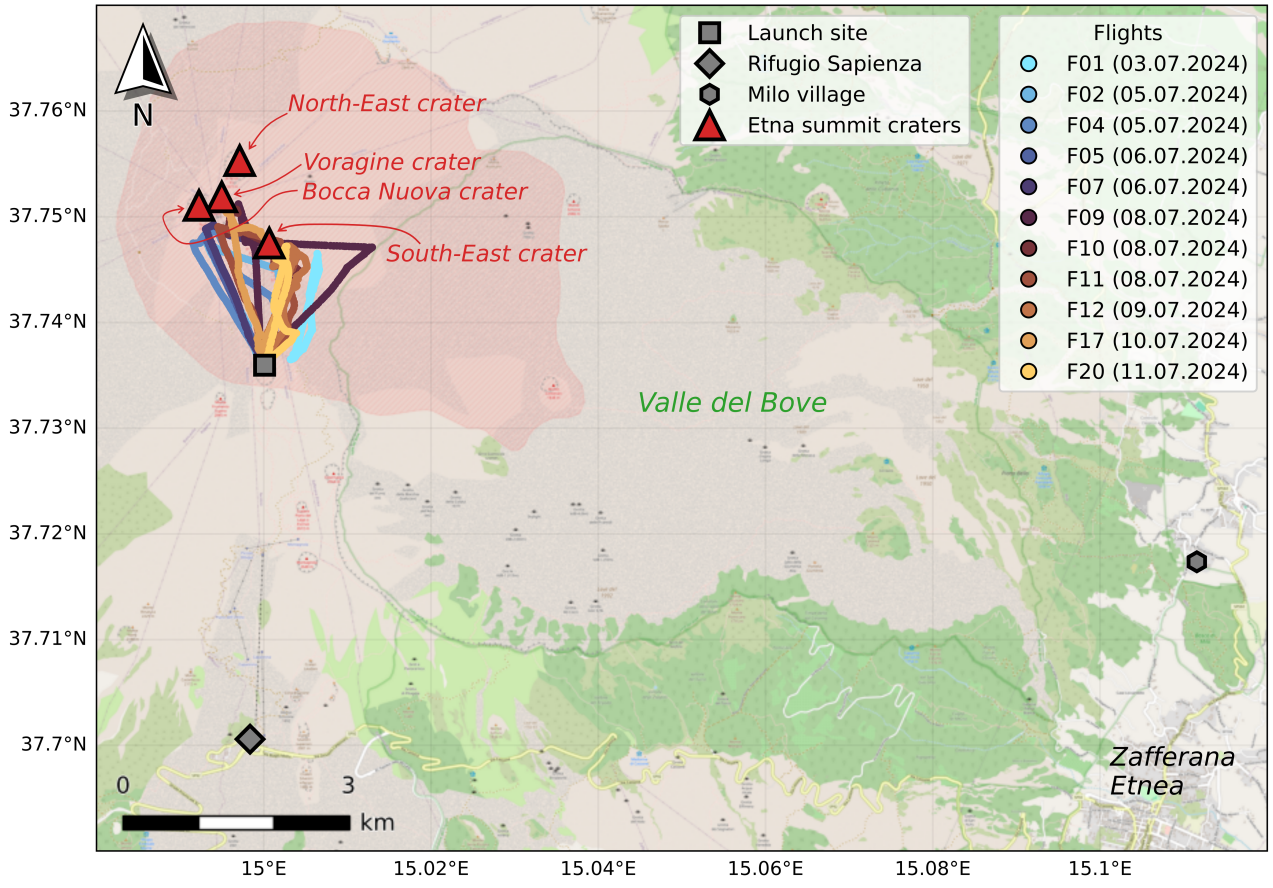

Figure 1. Overview of all flight tracks with deployment of active AirCore. The square indicates the location of the UAS launch site, the diamond and hexagon symbols mark the locations where the CRDS setup was located for post-flight analysis of AirCore samples. The samples from flight 17 and 20 were analysed at Milo village, all other samples at Rifugio Sapienza. Map data: ©OpenStreetMap contributors 2026. Distributed under the Open Data Commons Open Database License (ODbL) v1.0., https://www.openstreetmap.org/copyright/.

flight with cut-outs to ensure unhindered airflow across the CO_2 sensor and into the inlet. Note, that the air flow to the CO_2 sensor was passive, without using a pump. Values are thus not reliable and were only used for monitoring purposes during flights.

2.3 Post-flight analysis of AirCore samples

Post-flight analysis of AirCore samples was performed with a Picarro G2401 cavity ring down spectrometer (CRDS) measuring CO_2, CH_4, CO, and H_2O. The CRDS is a continuous flow gas analyser that enables measurements with a temporal resolution

https://doi.org/10.5194/egusphere-2026-1865
Preprint. Discussion started: 21 May 2026

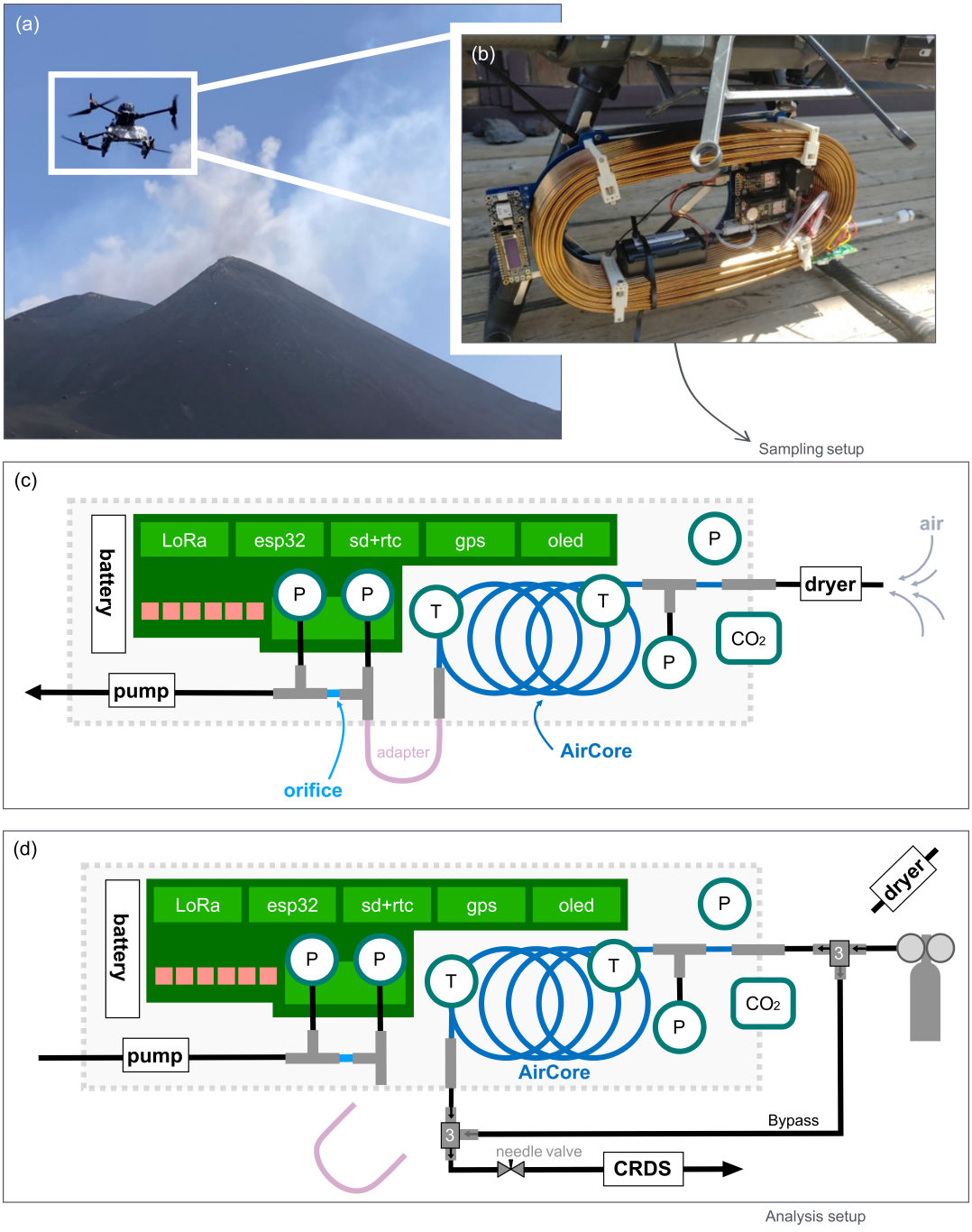

Figure 2. (a) Active AirCore attached to the UAS in operation at Mt. Etna. Picture (b) and schematic (c) of the AirCore setup for in-flight sampling. (d) The same as in (c) but for the analysis setup with bypass option and AirCore measurement mode. Technical details of the single components of the setup are listed in supplementary Table 1.

https://doi.org/10.5194/egusphere-2026-1865
Preprint. Discussion started: 21 May 2026

Table 2. Mole fraction values of the used tanks on WMO scales (CO_2: X2019, CH_4: X2004A, CO: X2014A).

	CO_2 [ppm]	CH_4 [ppb]	CO [ppb]
calibration gas	435.5 ± 0.1	2047.2 ± 0.5	166.2 ± 1.5
FG/PG	423.2 ± 0.1	1007.4 ± 0.9	1509.2 ± 27.3

of approximately 2–3 seconds. The necessary flow is generated by pushing the sample air through the AirCore tube with a so-called push gas (PG) and is kept constant by a needle valve installed upstream of the cavity (inlet mode). For the experiments described here, the PG was identical to the FG used to condition the tube before flights. In the following, the term PG will be used when the flow into the analyser is directly from the gas cylinder, and FG will be used when the flow is through the AirCore and the gas remaining in the AirCore tube from pre-flight preparation is analysed.

The CRDS instrument is able to measure CO_2 and CH_4 with a very high and CO with a good precision with typical precisions during field operations 0.03 ppm for CO_2, 0.2 ppb for CH_4, and 5 ppb for CO. Since a dryer was attached to the AirCore during sampling, water vapour, which the instrument also detects, is only used as an additional indicator to distinguish between air sample and FG or PG, or to detect contamination or leakages. The other trace gas measurements are reported as dry mole fractions on WMO scales (CO_2: X2019, CH_4: X2004A, CO: X2014A). They were calibrated using analyser specific parameters and a daily offset correction from measurements against a calibration tank for which mole fractions are listed in Table 2.

Because of the small inner diameter of the AirCore tube, mixing of sampled air inside the tube is slow, and the spatial distribution is preserved if the AirCore sample is analysed quickly after a flight. For practical reasons, namely weather protection and continuous and reliable power supply, the Picarro instrument could not be operated at the UAS launch site, but was installed at *Rifugio Sapienza* (37 °N 42’2”N, 14 °E 59’54”, 1910 m amsl, see Fig. 1). Samples could be analysed within 45–70 min after flights. For the two last flights of the series, the CRDS was set up at Milo village (37 °N 43’22”, 15 °E 7’0”, 757 m amsl), these analyses took place approximately 110 min after the flight. Detailed information on the delay between sampling and analysis (the so-called storage times) for each flight is listed in Table 1.

Figure 3 provides an example of the trace gas signals recorded by the CRDS instrument during the analysis procedure for one selected AirCore flight (F12, 9. July 2024). Eight different sections in the measurement time series are distinguishable. In the beginning (section 1), clean PG is measured, bypassing the AirCore. It is characterised by a high CO and low CH_4 mole fraction to make it easily distinguishable from ambient air (see Table 2 for exact values). After redirecting the gas flow to pass through the AirCore, a small amount of calibration gas is briefly observed (section 2). This occurs because the calibration gas was previously used to flush the line to the instrument during connection of the AirCore to the system. Following a peak in the mole fractions of all gases in section 3, which will be discussed in detail later, gas from inside the AirCore sampler is measured. At first, the FG remaining from before the flight is detected in section 4. After a transition in section 5 with elevated abundances in CO, CO_2, and H_2O, the actual AirCore air sample is analysed in section 6. In the sample, the CH_4 mole fraction remains almost constant at about 1960 ppb, reflecting the mole fractions in the free troposphere which are slightly below current ambient levels in the boundary layer. In the CO_2 mole fraction, several distinct features of volcanic plume air

https://doi.org/10.5194/egusphere-2026-1865
Preprint. Discussion started: 21 May 2026

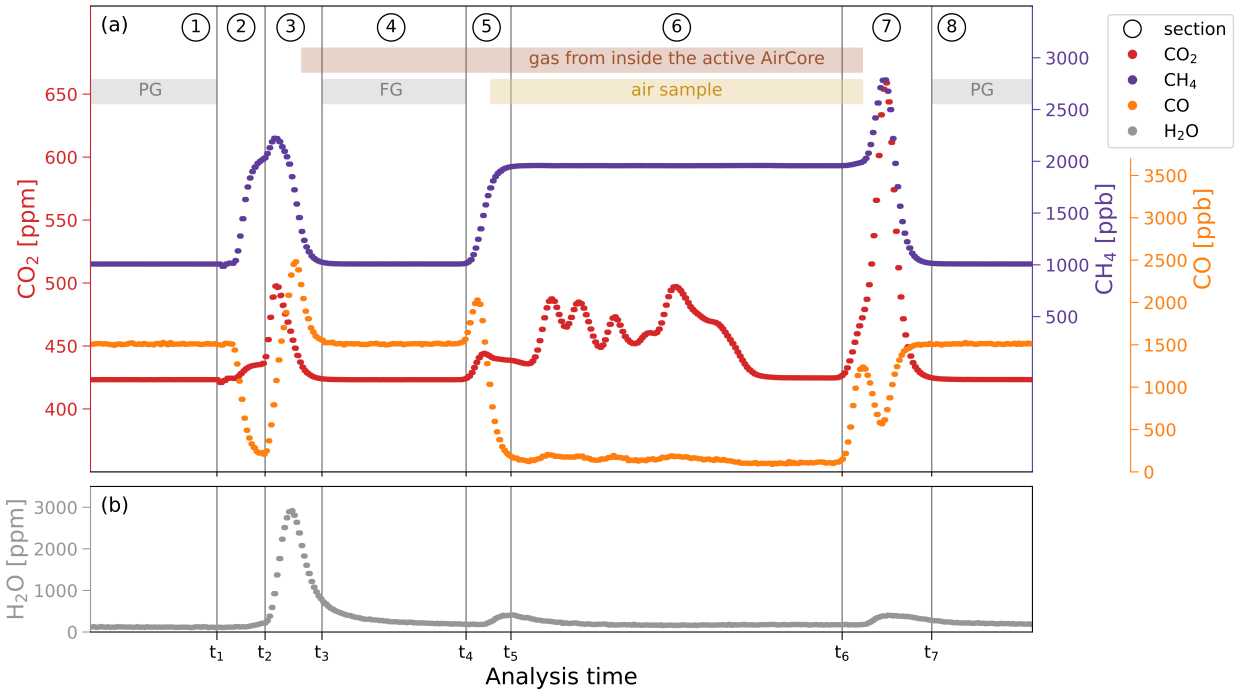

Figure 3. (a) CO_2, CH_4, CO and (b) H_2O signals recorded by the CRDS instrument during the analysis procedure for one selected AirCore flight (F12, 09.07.2024). Encircled numbers define sections of the time series as addressed in the text. Measurements of gas from inside the AirCore are highlighted by the the brown bar, the actual air sample is measured in section 6. The black vertical line between sections 1 and 2 marks switching from Bypass to AirCore measurement mode.

are visible, some of them accompanied by elevated CO. At the end of the measurement, again a feature of all three gases being elevated is visible in section 7, before the signal reaches the PG level again (section 8) and the measurement in AirCore mode was terminated to proceed with calibration tank measurements in bypass mode (not shown).

The distinct features in the gas mixture in sections 3 and 7 of the time series mark contaminations at the ends of the AirCore. They clearly originate either in or shortly behind the dryer or at the back of the AirCore coil. At these locations of the AirCore, plastic plug connectors are installed to couple the sampler to the analysis system. They were chosen because of their minimal weight and easy handling of attaching and detaching different tubing without additional tools. Nevertheless, they are not as inert and leak-tight as stainless steel vacuum connections, resulting in the observed contaminations. While the simultaneously occurring water vapour peaks (see panel b) indicate that the contamination is from ambient air, the height of the CO_2, CH_4, and CO peaks suggests that additional effects might be involved. We therefore tested the AirCore in various setups and conditions in laboratory and field experiments. We could rule out a source inside the coil for these features. We found that large pressure differences related to altitude changes between sampling and analysis in combination with PVC and/or Silicon tubing close to the connectors result in diffusion of highly elevated mole fractions of CH_4 and CO during storage time into the AirCore at the

https://doi.org/10.5194/egusphere-2026-1865
Preprint. Discussion started: 21 May 2026

ends. A similar explanation applies to the feature in section 5, as the gas mixture at the transition from FG to the air sample had a longer residence time in the area of the AirCore inlet and dryer before being pulled in when the pump was switched on.

Although the actual air sample itself is not significantly affected by these unexpected effects, as they do not occur during the typical pumping process, but only after a certain storage period, we recommend reconsidering the type of connectors and attachment tubing in the AirCore design to avoid them in future work by using fewer plastic components. This is even more true in such harsh and chemically active environments with special conditions like at Mt. Etna. As the features become more pronounced for larger altitude changes, it is advisable to avoid pressure differences during the storage of the AirCore before and after a flight. In consequence, the vertical distances between preparation point and landing point of the drone and analysis location should be as small as possible.

2.4 Retrieval of measurements, uncertainties and spatial resolution

To map the mole fractions from the AirCore sample analysis onto the flight trajectories of the UAS, the simplest way is to follow the approach proposed by Tong et al. (2023). Picarro measurement data, which are reported as a function of sample analysis time t^{analysis}, can be directly linked to the flight time t^{flight} and corresponding positional data. Provided that the sampling and analysis mass flow rates were both constant, the convolution can be done based on the fractions of the sampling and analysis times as the amount of moles remains unchanged.

$$t^{\text{flight}}(t^{\text{analysis}}) = t_0^{\text{sampling}} + \left(\frac{\Delta t^{\text{sampling}}}{\Delta t^{\text{analysis}}}\right) \cdot \left(t^{\text{analysis}} - t_0^{\text{analysis}}\right) \tag{1}$$

For our deployment of the active AirCore at Mt. Etna over large vertical ranges, the assumptions underlying this linear mapping equation are not completely fulfilled. Although the analysis flow rate was kept constant by using the needle valve in the Picarro setup, the assumption of a constant sampling flow rate only applied during parts of each UAS flight. In addition to the predominant sampling at approximately steady cruise altitude, each flight is characterized by shorter transient phases during ascent and descent, accompanied by significant pressure changes influencing the sampling flow. Supplementary Fig. S2a shows an exemplary flight altitude time series. To prevent erroneous distortion of the mapping, it is necessary to apply a correction for these effects.

As presented by Andersen et al. (2018) and the well-established procedure for passive AirCore altitude attribution (e. g. Membrive et al., 2017; Wagenhäuser et al., 2021), the projection of the measurements onto the flight track for such active AirCore flights with variable flows can be performed based on the calculation of the sampling fill fractions $n_{\text{rel}}(t^{\text{flight}})$ inside the AirCore, representing the relative amount of sampled gas at a given time. Following the concept of Wagenhäuser et al. (2021) adapted for active AirCore, the retrieval is done via a three-stage process:

(i) The sampling of air during the UAS flight is calculated based on the net-sampling flow.

(ii) The start and end times of the AirCore measurement are identified within the analyser time series.

(iii) Sampling and analysis can be matched based on the molar amount.

https://doi.org/10.5194/egusphere-2026-1865
Preprint. Discussion started: 21 May 2026

For the first step, we propose a simplified 'inflow–outflow' model to calculate the net-sampling flow f^{net} along the flight trajectories, taking into account air being pulled in by the pump (f^{pump}) and the flow $f^{\text{volume effect}}$ caused by the pressure-related change in coil volume ΔV^{coil}:

$$f^{\text{net}}(t^{\text{flight}}) = f^{\text{pump}}(t^{\text{flight}}) + f^{\text{volume effect}}(t^{\text{flight}}) = f^{\text{pump}}_{\text{nominal}} \cdot \left(\frac{p(t^{\text{flight}})}{p_0}\right) + \left(\frac{\Delta V^{\text{coil}}(t^{\text{flight}})}{\Delta t^{\text{flight}}}\right) \tag{2}$$

Hereby, the actual inflow from pulling air through the AirCore with the micro pump f^{pump}, i. e. the pressure-dependent critical flow through the orifice, can be determined from the nominal sampling flow rate under standard conditions ($f^{\text{pump}}_{\text{nominal}}$, 22 sccm in this case), corrected for the current ambient pressure $p(t^{\text{flight}})$. The inflow or outflow resulting from the contraction or expansion of the air inside the coil is caused by the pressure dependence of the coil volume V^{coil}.

$$V^{\text{coil}}(t^{\text{flight}}) = V^{\text{coil}}_{\text{nominal}} \cdot \left(\frac{p(t^{\text{flight}})}{p_0}\right) \tag{3}$$

This approach is a first order approximation to correct for pressure changes along the flight path, but does not take into account temperature changes which are considered negligible.

Finally, the amount of air sampled $n(t^{\text{flight}})$ can be derived from the cumulative net-sampling flow divided by the coil volume:

$$n(t^{\text{flight}}) = \left(\frac{\sum_{i=1}^{t^{\text{flight}}} f_i^{\text{net}}}{V_{\text{coil}}(t^{\text{flight}})}\right), \tag{4}$$

and the sampling fractions $n_{rel}(t^{\text{flight}})$ are the ratio of this quantity and the total sampled amount:

$$n_{\text{rel}}(t^{\text{flight}}) = \left(\frac{n(t^{\text{flight}})}{n_{\text{total}}}\right). \tag{5}$$

Due to the constant flow rate of the analyser, the relative amount of measured gas $m_{\text{rel}}(t^{\text{analysis}})$ is defined as the ratio of the elapsed analysis time to the total duration of the analysis. Finally, matching $n_{\text{rel}}(t^{\text{flight}})$ to $m_{\text{rel}}(t^{\text{analysis}})$ yields the attribution of the trace gas measurements and the positional data. This approach can, in contrast to the linear mapping in Eq. 1, account for the non-uniform filling of the active AirCore, including undersampling during the initial ascent, potential sample loss due to temporarily negative net flows, and oversampling during the descent phase. Figure S2a summarises the components of the proposed flow model and highlights the differences between the sampling fraction based and the linear approach, expressed as a temporal attribution offset (panel b) and in terms of the CO_2 mapping results (panel c).

The procedure to identify the exact air sample analysis time within the Picarro measurement time series is the following: The transitions preceding and following the uncontaminated air sample (section 6 in Fig. 3) are characterised by distinct gradients in the different species. These features are used to determine the times corresponding to the end and beginning of the sampling time. Taking into account diffusion during storage time and mixing in the analyser cell, the start of the air sample segment is

https://doi.org/10.5194/egusphere-2026-1865
Preprint. Discussion started: 21 May 2026

assumed to be the midpoint of the CH_4 mole fraction transition from clean FG to typical ambient values. For the last sampled end of the air sample, this criterion needs to be adjusted, as the pressure increase of roughly 100 hPa between the launch site and the measurement site caused more ambient air and/or air from the dryer to be pushed into the sample after the flight. This can be compensated for using the corresponding CO contamination. We chose the point in time corresponding to the first appearance of 50 % of the CO values expected in PG as the best estimate for the sample end. To account for the somewhat arbitrary selection of these times, we repeated the procedure with slightly shifted definitions (25 % and 75 % of each transition) to estimate uncertainties for the determination of the start and end point. The resulting timing uncertainties in mapping the measurements onto the flight track are summarized in Table 3 along with corresponding maximum possible displacements in each direction. They are always less than 140 m, but strongly depend on the UAS velocity and thus vary significantly along the flight track. Most of the time, they are in the range of 2–10 m.

The effective spatial resolution of the active AirCore results from (i) molecular diffusion and Taylor dispersion inside the sample, (ii) analyser averaging effects, (iii) GPS uncertainties, and (iv) the speed of the UAS. To derive the spatial resolution of the measurements, we followed the method presented in detail by Andersen et al. (2018). For the data from the campaign at Mt. Etna, typical values of the spatial resolution for the horizontal direction range from 24.9 to 91.0 m and for the vertical direction from 4.3 to 22.1 m. Information for each flight considering flight-specific UAS movement patterns and storage times are included in Table 3 and shown graphically in supplementary Fig. S3. They will be discussed further in section 3.1.

The key parameter for evaluating the averaging effect of the AirCore technique is the effective measurement volume, determined by sample smearing inside the CRDS cavity (constant effective volume: 5.5 cm^3) and the diffusion volume which mainly depends on coil geometry and storage time. From its ratio with the previously discussed sampling flow we get a characteristic time, representing the sampling interval that corresponds to a single measurement and being interpreted as uncertainty of the measurements. To derive the spatial resolution, this effective time resolution is multiplied with the average flight speed during this period. Although the GPS uncertainty of 2.5 m in general has a negligible effect for the effective spatial resolution, it might be a significant additional factor in cases with long standstill of the UAS at a single location when the velocity-related part of the spatial uncertainty becomes small.

Note that during data processing the parts of the selected sampling period within the analysis time series affected by mixing with FG or including potential contamination from the ends of the AirCore were cautiously flagged. Making use of the flight pattern with the UAS starting and landing in background-like conditions in the launch area and taking some time flying to and from possible plume encounters in between, we apply the criterion of first/last appearance of low CO (< 200 ppb) to do so (times t_5 and t_6 in Fig. 3, see also Fig. 4).

2.5 The Multi-GAS instrument

Multi-component Gas Analysing Systems (Multi-GAS) are used to measure various target gases in volcanic plumes (Aiuppa et al., 2005; Shinohara, 2005; Salas-Navarro et al., 2022). They are easily portable and light, which makes them logistically very interesting when working at the top of a volcano, nowadays even onboard a UAS (James et al., 2020; Liu et al., 2019; Karbach et al., 2022). Moreover, they enable *in situ* real-time continuous measurements of the plume composition which makes

https://doi.org/10.5194/egusphere-2026-1865
Preprint. Discussion started: 21 May 2026

Table 3. Overview of spatial resolutions and uncertainties for each individual active AirCore flights for horizontal (↔) and vertical (↕) direction. Values for the vertical direction are shown in italics. They represent median values. For the UAS velocity also the maximum value is listed. These velocities were only reached for very short periods of time but are listed as an indication for the maximum variability. Spatial resolution statistics are also shown in supplementary Fig. S3.

flight code	effective time resolution [s]	uncertainties start/end [s]	direction	max. UAS velocity [ms^{-1}]	median UAS velocity [ms^{-1}]	spatial resolution [m]	max. possible displacement [m]
F01	22.8	$< \pm 5.0$	↔	26.07	0.35	29.8	131.3
			↕	*7.97*	*0.21*	*21.6*	*40.1*
F02	22.6	$< \pm 5.2$	↔	18.63	0.22	32.8	96.4
			↕	*8.70*	*0.05*	*4.3*	*45.0*
F04	23.4	$< \pm 7.4$	↔	18.27	2.21	91.0	135.8
			↕	*8.20*	*0.25*	*11.3*	*60.9*
F05	21.6	$< \pm 7.4$	↔	15.34	1.60	70.1	113.5
			↕	*10.29*	*0.50*	*22.1*	*75.5*
F07	22.5	$< \pm 4.6$	↔	17.71	0.44	44.4	82.2
			↕	*16.01*	*0.34*	*14.9*	*74.2*
F09	22.0	$< \pm 7.4$	↔	17.42	0.50	46.2	129.4
			↕	*7.20*	*0.21*	*6.3*	*53.5*
F10	22.6	$< \pm 7.5$	↔	18.32	0.23	37.1	137.0
			↕	*8.04*	*0.32*	*5.6*	*59.8*
F11	22.6	$< \pm 5.1$	↔	18.41	0.44	57.8	94.6
			↕	*6.52*	*0.2*	*21.6*	*33.4*
F12	22.4	$< \pm 4.7$	↔	19.04	0.39	44.0	88.7
			↕	*7.24*	*0.13*	*8.1*	*33.6*
F17	24.3	*	↔	32.16	0.28	24.9	
			↕	*16.40*	*0.12*	*9.5*	
F20	24.5	*	↔	18.11	0.31	30.0	
			↕	*6.83*	*0.16*	*5.2*	

* The estimation of matching uncertainties, as defined in section 2.4, is not reliably applicable to F17 and F20, as the larger pressure change between sampling and analysis sites causes more ambient air to enter the AirCore in the meantime. However, the time series plots for both flights in supplementary Fig. S13 and Fig. S14 indicate a clearly higher uncertainty in the determination of the start and end points of up to ± 60 seconds.

https://doi.org/10.5194/egusphere-2026-1865
Preprint. Discussion started: 21 May 2026

it possible to adjust flight patterns almost immediately based on observed trace gas mole fractions, complementing the UAS optical camera information. In total, three different sensor packages were part of the UAS payload during the campaign. In the following we focus on the package that was deployed most frequently with a total of 17 flights covered, including most of the flights when an active AirCore sample was collected, except for flight F01 and F02.

The Multi-GAS sensor package that was used has been described in detail previously by Karbach et al. (2022). It was controlled with an ESP32 board and included GPS and telemetry modules as well as sensors for environmental parameters. It provided NDIR sensor data of CO_2 mole fractions (in this study a Senseair K30 FR is used instead of an ELT S-300) and electrochemical sensor measurements for SO_2 (Alphasense SO2-B4). Real-time monitoring of the sensor observations with a tablet computer in the field allowed an immediate assessment of the plume positions. Continuous air flow over the sensors was ensured with a micro pump (First Sensor, T5-1HE-03-1EEB). Following the procedure described in Karbach et al. (2022), the calibration and the response time correction of the specific sensors were conducted with different mixtures of CO_2 and SO_2 of known mole fractions mixed and stored in Tedlar gas sampling bags. The experimentally determined response times were $\tau_1/e = 13$ s for the CO_2 sensor, and $\tau_1/e = 10$ s for the SO_2 sensor, respectively.

2.6 Data processing: plume detection and calculation of mole fractions enhanced from background

Potential plume encounters during flights were identified from the measurement time series relying on the active AirCore CO_2 mole fractions using a simple peak detection algorithm. Hereby, a minimum peak prominence of 1 ppm (signal to noise ratio greater than 3) and a minimum peak width at half their relative height of 15 seconds were used as filter criteria. In addition, a minimum horizontal distance of 30 seconds to the next neighbouring peaks was required to define a peak as the centre of an independent possible plume event. The beginning and end of the plume were defined as the points in time corresponding to the peaks shoulder values at half the relative height. To assess whether a volcanic plume was crossed, the detected events were subsequently compared to the SO_2 sensor data if available. The results are discussed in Sec. 3.2. Due to the lack of sufficiently high-quality SO_2 sensor data for some flights and uncertainties in merging the data sets, direct identification based on SO_2 was not suitable.

To use the abundance and mole fraction ratio of different species degassing from the volcanic vents as indicators of activity and to understand plume chemistry, mole fraction enhancements need to be calculated relative to background conditions. Background mole fractions for each individual flight were calculated as the average of the lowest quartile (< 25 % percentile) of each the CO and CO_2 measurements. These correspond almost exclusively to the air sampled at the very end of each flight, as we tried to end each UAS flight with a hovering phase close to the starting area in more than a kilometre distance to the active Etna craters. These values reflect local short-term background conditions and might not be representative on a larger scale, because the huge Etna degassing might cause an overall elevated background in comparison to non-polluted sites in the region. Moreover, other near-site emissions, for example from vehicles might play a role. For example, CO_2 measurements from Lampedusa (LMP, about 200 km south-east of Sicily, ICOS station; ICOS Research Infrastructure et al., 2025) show an average mole fraction of 419.9 ± 2.2 ppm during the time of the campaign in July 2024, which is roughly 2–10 ppm lower than the background values from our flights. Fig S1 summarises the local background mole fractions for each flight and

https://doi.org/10.5194/egusphere-2026-1865
Preprint. Discussion started: 21 May 2026

illustrates the differences to the measurements at the LMP site, which can be interpreted as regional background values. In contrast to local background CO_2, which is quite uniform around 425 ppm (± 1 %), local background CO between the flights is more variable with absolute values ranging between 100 ppb and 160 ppb. This is expected and can partly be attributed to general tropospheric CO variability associated with different weather conditions and variable air masses transported to Mt. Etna. However, the combination of such high variability in the background and background identification close to a potentially strong, fast-changing emission source introduces significant uncertainties in the calculation of the enhanced CO mole fractions compared to the much more robust CO_2.

Keeping these limitations in mind, the enhanced mole fractions due to Mt. Etna emissions were calculated above the local background and averaged for each plume event. From these plume mean mole fractions, tracer-tracer ratios are calculated for each event.

3 Results and discussion

3.1 Active AirCore and sensor performance

CO_2 was measured simultaneously using both the Multi-GAS sensor package and the active AirCore, with each technique exhibiting specific advantages and challenges. Figure 4a shows the comparison of the CO_2 measurements from AirCore and from the Multi-GAS NDIR sensor as a function of flight time for flight F12. Note that the datasets are presented on separate y-axes, which are shifted but not different in scaling. This already points at a key limitation of the NDIR sensor data. Although the sensor was sensitivity calibrated before and after the campaign there is an offset in the absolute mole fractions compared to the high-accuracy post-flight analysis of the AirCore sample. This known issue can be associated with the sensor drift and is usually corrected for by applying an additional daily offset correction based on an estimate of the background mole fractions (Karbach et al., 2022). This highlights how much more accurate measurements can be provided by the active AirCore technique.

Regarding the sequence and distinctiveness of individual patterns, the CO_2 time series from the different devices agree very well. Keeping in mind the small effect of the sensor response time and the uncertainty in the assignment of the CRDS measurements to the sampling time, the comparison confirms that the AirCore retrieval method performs well, as the positions of extrema differ by only a few seconds between the two independent datasets.

The NDIR sensor, with a detection rate of approximately 1.2 Hz, offers higher temporal resolution than the AirCore method, where the effective time uncertainty and resolution of an individual measurement — depending on storage time and analyser averaging — and not the CRDS analyser measurement rate are relevant. For flight F12, this effective time is approximately 22 s (see also Table 3), visualized by the red horizontal error bars in Fig. 4a. The averaging effect of the AirCore technique is present, but not strongly pronounced. The shape of the individual features is preserved and only slightly reduced and smeared out compared to the high-resolution sensor data.

Focusing on the UAS speed during flight F12 presented in Fig. 4b, it becomes clear that the trajectory is characterised by fast acceleration and deceleration and changes of direction. In particular directly after take-off and when flying back to the starting

https://doi.org/10.5194/egusphere-2026-1865
Preprint. Discussion started: 21 May 2026

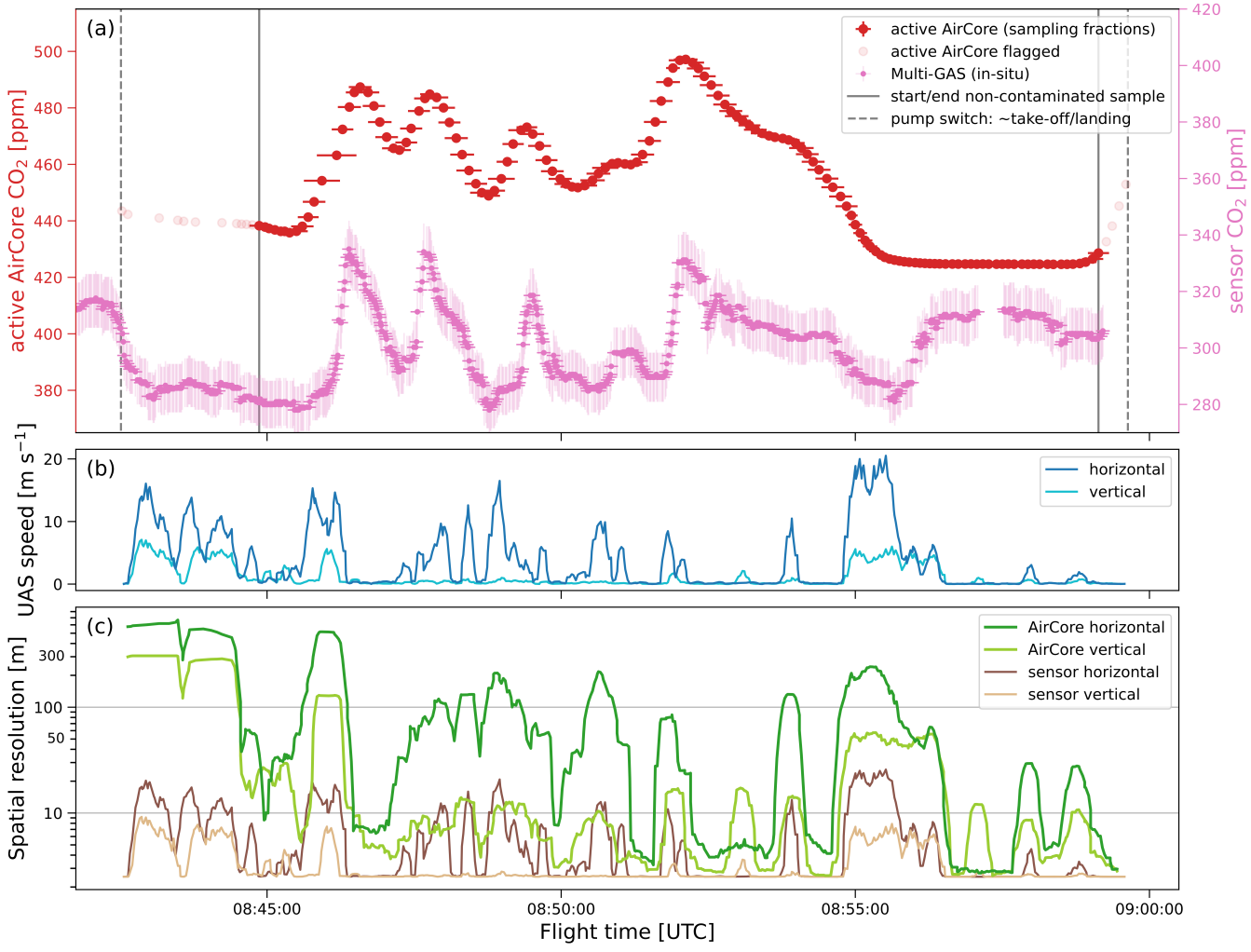

Figure 4. (a) CO_2 measurements during flight F12 (09.07.2024) from the active AirCore technique (left y-axis) and the Multi-GAS sensor package (right y-axis) alongside the drone vertical and horizontal speed (b) and the effective spatial resolution of each device (c). Note that vertical error bars of the active AirCore measurement are smaller than symbol size. Horizontal error bars reflect the averaging kernel of the AirCore which is larger than the displacement uncertainty. Vertical dashed lines in panel (a) indicate the times when the pump was switched on and off prior to and after the flight.

area with high velocities, a significant effect on the NDIR sensor is observed, manifesting as jumps followed by a distinct drift (shortly after 8:40:00 UTC and 8:55:00 UTC).

Also for the spatial resolution, shown in Fig. 4c for both devices, a clear dependency on the flight pattern is evident. While the spatial resolution of the sensor is more closely related to the current UAS speed and is always below 40 m in the horizontal and 15 m in the vertical direction, the spatial resolution of the AirCore depends on the drone movement over a longer period of time

https://doi.org/10.5194/egusphere-2026-1865
Preprint. Discussion started: 21 May 2026

and the net-sampling flow. Maximum values with more than 500 m in the horizontal and up to 300 m in the vertical direction are reached shortly after launch, when a significantly reduced net-sampling flow or even temporary sample loss occurred due to the fast ascent. In contrast, the spatial resolution is better than 30 m and 10 m for phases of background sampling prior to landing. During plume encounters, the spatial resolution is variable typically ranging between 10–100 m horizontally and 5–20 m vertically. Since we calculated the spatial resolution simply based on the UAS flight speed and do not account for changes of direction or complex flight patterns, the true spatial resolution might be partly substantially below the values reported here. It should be interpreted as the maximum possible distance travelled during a given time interval. Moreover, the metric is somewhat misleading as we sometimes tried to stay in a plume and therefore tracked a specific air mass, so that a Lagrangian perspective would be more useful to interpret the measurement results.

Beyond the case study of flight F12, comparisons of CO_2 from the different techniques across the other flights (see Fig. S4) confirm the main findings described above while revealing the sensor system's higher sensitivity to disturbances. Significant noise in the measurements from the Multi-GAS CO_2 NDIR sensor occurs during approximately half of the flights, which allows the detection of only the largest peaks and complicates the interpretation of the data (e. g. for flights F07 and F11). Although additional post-processing steps (e. g. smoothing, see black curve in Fig. S4) could somewhat improve the data quality, the lower reliability - especially when no comparison measurements are available - remains problematic. The higher failure rates of the sensors are most likely due to a combination of unfavourable surrounding conditions and the performance of the mini-pump, which may not have been sufficient to maintain a consistently high flow rate towards the sensor. Problems were observed more frequently in weather with stronger or highly variable winds, as well as during unsteady flight patterns characterised by higher UAS speeds and frequent, quick changes in direction. The sensors are susceptible to rapid pressure fluctuations, especially occurring as a result of high vertical speeds. Thus, high vertical speeds should only be used during flight phases when this is acceptable and flight patterns should be planned accordingly.

Despite these limitations, the advantages of the sensors are obvious as they are light-weight, relatively inexpensive and easy to operate. In addition, we have to keep in mind that the measurements were conducted under extreme conditions (over 3000 m altitude, chemically active and particle-rich volcanic plume air), putting extreme demands and stress on the components. Of course, the same applies to the AirCore. The harsh environment and strong forces acting on the setup during flights were also likely the reason for some brief power cuts that occurred during F05 and F07, causing a temporary failure of the AirCore pump and resulting in a gap in the sampling. To further reduce the risk of such a scenario in future work, it would be advisable using a more stable battery mount and connectors that can withstand extreme flight forces. Additionally, improving the shielding of electronic components against outside air would be beneficial, although this would likely adversely impact payload manageability and flight duration. Although pressure fluctuations, particularly during the ascent, are not ideal for the AirCore filling process and complicate the mapping of the measurements, the combination of a strong pump and a critical orifice as well as the novel sampling fraction based retrieval effectively compensates for this effect. Nevertheless, further experiments or modelling of such influences would certainly be valuable, as has already been conducted by Tans (2022) for the passive AirCore. Overall, we recommend adjusted flight paths with less rapid movements of the UAS, smoother changes in direction and longer sampling under quite homogeneous conditions instead of fast changes. In this context, the applied approach combining AirCore sam-

https://doi.org/10.5194/egusphere-2026-1865
Preprint. Discussion started: 21 May 2026

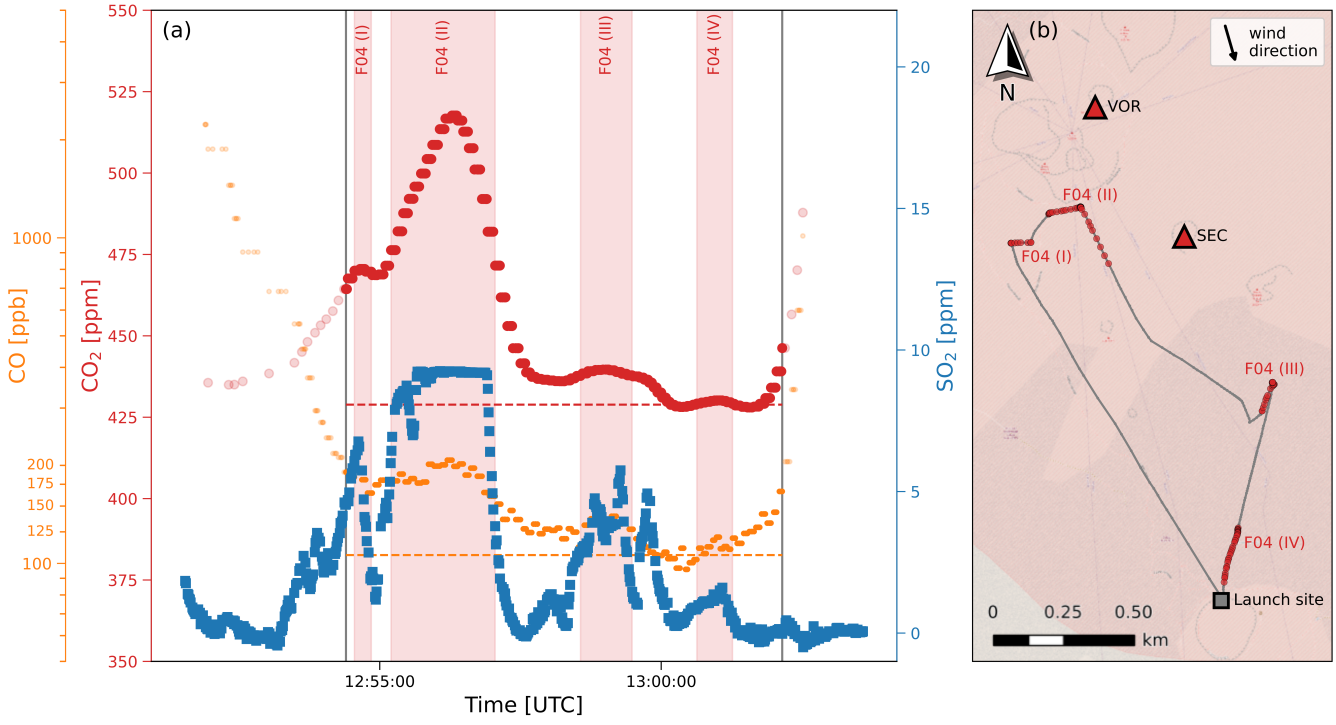

Figure 5. Plume identification in the active AirCore sample based on CO_2 signal in comparison to SO_2 sensor measurements (a) and locations of the possible plume encounters along the flight track (b) for F04. The potential volcanic plume events are highlighted in red in both panels. Horizontal dashed lines in the time series plot show local background values of the species and vertical lines frame the period of non-contaminated measurements. For all other flights, analogous figures are included in the supplementary information (Figs. S5–S14)

pling with simultaneous real-time monitoring using low-cost sensors has proven extremely useful in enabling precise plume measurements and plume identification.

3.2 Evaluation of plume events

In total, using the algorithm based on the CO_2 measurements as described in section 2.6, 38 possible plume encounters were identified during the eleven active AirCore flights. Before analysing the chemical composition and signature of the volcanic plume air, these plume candidates are further differentiated into actual plume events and probably contaminated or erroneously assigned events to avoid misinterpretation. Fig 5a illustrates the results of this evaluation exemplary for flight F04 showing the CO_2 measurements next to the SO_2 sensor readings. For other flights, see Figs. S5–S14 of the supplementary information.

The primary source for non-plume CO_2 peaks which are not related to volcanic air are most likely effects at the AirCore inlet and the dryer shortly after the pump is activated. Thus, the first part and any peak occurring within this sample measurement phase marked as potentially contaminated based on the CO mole fraction (cf. Sec. 2.4) should be interpreted with caution (e.g. feature $F17_{(I)}$ in Fig. S13 where no corresponding SO_2 signal above the background level was detected, so it is unlikely that a

https://doi.org/10.5194/egusphere-2026-1865
Preprint. Discussion started: 21 May 2026

fresh plume was crossed). For flight F04, all four plume candidates were identified during the remaining flight period, when the CO_2 and SO_2 generally correlate very well, indicating that the sampling actually took place inside a volcanic plume. This is also consistent with the locations of the relevant measurements highlighted in Fig. 5b, which were close to and downwind of the vent positions (VOR for $F04_{(I)}$ and $F04_{(II)}$, SEC for $F04_{(III)}$). The significantly weaker event $F04_{(IV)}$ towards the end of the flight and at a greater distance from the craters might have been a more aged and mixed plume.

Focusing on the SO_2 readings, it should be noted that the sensor reached saturation for mole fractions above 10 ppm due to ageing. As already discussed in the previous chapter on the AirCore vs. CO_2 sensor comparison, minor discrepancies in the expected match between the SO_2 sensor and AirCore can be attributed to uncertainties in the retrieval procedure in combination with the sensor response time or differences in the time resolutions causing e. g. a slight delay of the time series relative to each other. Consequently, the signature of some short-term events might be somewhat biased. This is particularly strong for flights F17 and F20 (cf. Figs. S13 and S14), AirCore samples of which were analysed at Milo village. The longer travel distance between the sampling and the analysis site resulted in a longer storage time, i. e. larger diffusion effects, and because of the greater altitude difference also in a larger contamination at the end of the AirCore sample because of the pressure difference during sample transport. The algorithm for the detection of the sample end did therefore not work as well as for the other flights, resulting in a larger uncertainty of the matching of the sample onto the flight track. Nevertheless, the combined datasets allow for a profound analysis of plume composition and $\Delta CO/\Delta CO_2$ ratios which rely only on data from the AirCore are not affected by this.

For the entire campaign, these considerations and quality control assessments led to rejection of four potential plume events because they can be traced back to a contamination with high confidence, whereas the status of another four events remained unclear. The residual 30 Etna plume encounters are analysed in more detail in the next section. To compare different plume crossings, we calculated the average and standard deviation of all measured parameters during the plume sampling intervals. Note that these statistics are sensitive to the exact definition of the plume events.

3.3 Trace gas distribution at Mt. Etna

Figure 6 shows the correlation between the average mole fractions of SO_2 and CO_2 during the different Etna plume encounters (blue dots). Compared to the black-bordered rectangular region indicating background conditions (lower left corner, uncertainties in gray), it becomes apparent that both species are strongly enhanced within each plume. Although a considerable variability is evident, the performed ordinary distance regression (ODR) confirms a correlation between the enhancement of both species. The SO_2 mole fraction rises by approximately 1.1 ppb for each 10 ppm increase in CO_2. The average $\Delta CO_2/\Delta SO_2$ ratio derived from the enhanced mole fractions over background is (10.1 ± 9.3) ppm ppb^{-1}. This is within the range of CO_2/SO_2 plume ratios of 0.6-–30 ppm ppb^{-1} reported by Shinohara et al. (2008) from their measurements at the different Etna craters using ground-based Multi-GAS instrumentation in 2005 and 2006. Aiuppa et al. (2008) reported slightly lower bulk mean ratios of (5.7 ± 1.1) ppm ppb^{-1} based on Licor NDIR spectrometry observations of CO_2 and electrochemical sensor measurements of SO_2 as did Voigt et al. (2014) with 5.2 ppm ppb^{-1} during their probing of plume evolution with a research aircraft.

https://doi.org/10.5194/egusphere-2026-1865
Preprint. Discussion started: 21 May 2026

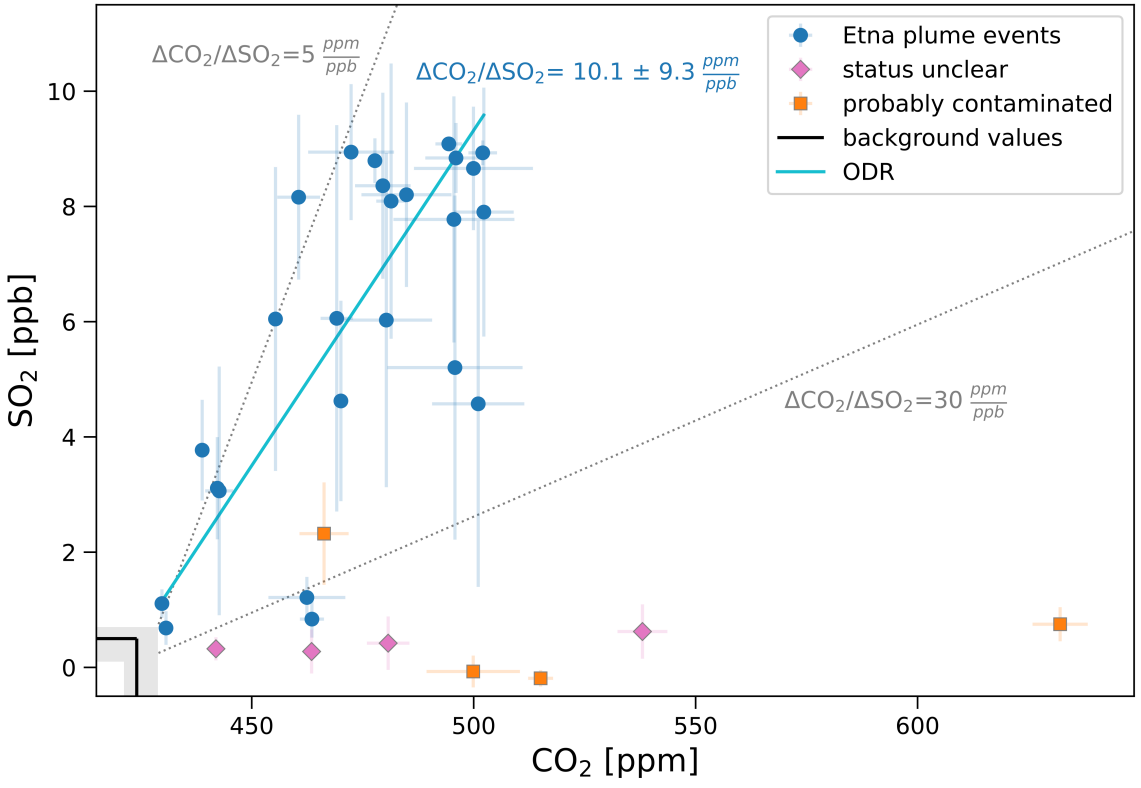

Figure 6. SO_2 vs. CO_2 correlation during plume encounters. The black lines mark typical background conditions and orange data points are identified events from probably contaminated parts of the time series. Symbols represent mean values during the encounters and error bars its standard deviation. The solid blue line represents an orthogonal distance regression (ODR) to the plume events to guide the eye. Dotted lines indicate the range of 5–30 ppm ppb^{-1} into which most values from the literature fall.

As the ratio changes also over time correlated to activity (e.g. Aiuppa et al., 2007), in Fig. 6 the range of 5–30 ppm ppb^{-1} is indicated by the dotted lines to give an estimate of common values from literature.

While the CO_2/SO_2 ratio is a commonly used metric to monitor volcanic activity, observations of the CO/CO_2 redox pair in volcanic plumes are very limited. The newly obtained measurement data from active AirCore sampling provide a unique opportunity to study plume chemistry and interactions with atmospheric air. Figure 7a shows the mole fraction enhancement ratio $\Delta CO/\Delta CO_2$ observed in the Etna crater region with gray shaded areas indicating periods of eruptive activity at the VOR crater (see Calvari and Nunnari (2024) and Bonaccorso et al. (2025) for details on the sequence of volcanic activity). The different symbols highlight which vent was located upwind of the UAS position during the plume encounter. Note that plume events with a standard deviation of the enhanced mole fractions exceeding the average value for one of the species were not

https://doi.org/10.5194/egusphere-2026-1865
Preprint. Discussion started: 21 May 2026

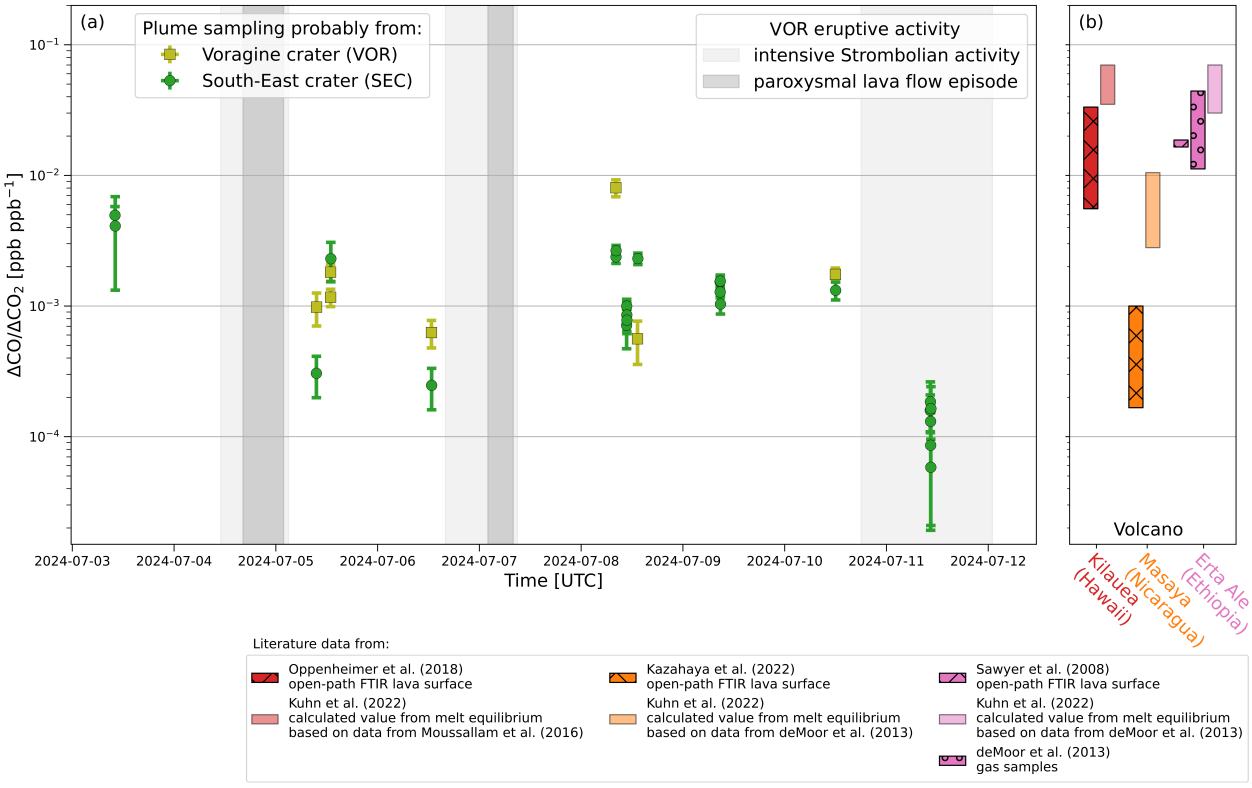

Figure 7. (a) $\Delta CO/\Delta CO_2$ for all plume encounters during active AirCore flights at Mount Etna. Different colours and symbols indicate the crater vent located downwind of the UAS position during plume sampling. The shaded areas indicate time periods of eruptive activity at the Voragine crater within the campaign period (Calvari and Nunnari, 2024; Bonaccorso et al., 2025). (b) Overview of literature $\Delta CO/\Delta CO_2$ values from three different volcanos for comparison. Either measured at lava lakes using open-path Fourier transform infrared spectroscopy (FTIR), within fumarole gas samples or derived from calculations based on melt temperature and oxygen fugacity from melt inclusion and matrix glass samples.

considered. During the campaign phase in July 2024, $\Delta CO/\Delta CO_2$ varied strongly between $8 \cdot 10^{-3}$ and $5 \cdot 10^{-5}$ ppb ppb^{-1}. Although fairly robust enhancement ratios are observed during flights with multiple encounters of a particular vent's plume over timescales of a few minutes, there are noticeable differences between individual flights, even on the same day (e. g. F09, F10 and F11 on 08.07.2024, with approximately 3 hours between each flight).

The differences in $\Delta CO/\Delta CO_2$ between the VOR and SEC plumes during the same flight are particularly striking. For example during F11 on 8. July 2024, when sampling downwind of both vents in quick succession, the SEC plume showed a five time higher ΔCO mole fraction than the VOR plume, while ΔCO_2 was similar (see Fig. S11). A reduced $\Delta CO/\Delta CO_2$ ratio was observed in the SEC plume during intense eruptive activity at the VOR crater on 11.07.2024. At the time of sampling, activity was characterised by near-continuous Strombolian explosions and was followed by lava fountains within the next hours.

https://doi.org/10.5194/egusphere-2026-1865
Preprint. Discussion started: 21 May 2026

In parallel, we measured strongly enhanced local background CO mole fractions of more than 150 ppb. This might somewhat distort or mask changes of the ratio inside the SEC plume and the entire crater region was dominated by the superimposing emissions originating from the VOR eruption.

Overall, we could not identify a simple connection between the ratio's variability and the volcanic activity. It is much more likely that the differences between individual vents and also the inter-flight variation are due to a complex interplay of various factors: In addition to temporal changes in the gas emission rate and composition, potentially associated with magma (gas) temperature or the volcanic conduit system, the meteorological conditions affecting plume dilution and mixing, as well as chemical ageing of the plume due to oxidation processes or heterogeneous interaction with volcanic ash and aerosol, may play an important role. Although we were unable to identify a clear dependence of the $\Delta CO/\Delta CO_2$ ratio on, for example, the distance from the vent (cf. Fig. S15) used as a proxy for plume age, the low ratios might point at fast oxidation processes happening between degassing and plume sampling.

Several studies focusing on different volcanoes have reported systematically higher $\Delta CO/\Delta CO_2$ mole fraction ratios mostly between 10^{-1} and 10^{-3} ppb ppb^{-1} (see Fig. 7b), both for ratios predicted indirectly from melt equilibrium (Kuhn et al., 2022) and those obtained from lava lake (Sawyer et al., 2008; Oppenheimer et al., 2018; Kazahaya et al., 2022) or gas sample measurements (de Moor et al., 2013). Furthermore, recent modelling studies by Roberts et al. (2019) or Kuhn et al. (2022) showed that plume composition, for example with respect to CO, can be substantially altered already within seconds after emission. In this context, the unique high-quality CO and CO_2 dataset presented here, and obtained using the innovative active AirCore technique provides important observational data to evaluate such findings and to support further studies on this topic.

4 Conclusions

Air sampling with the still new active AirCore technique allows to sample small amounts of air spatially resolved on flexible and well-controlled trajectories. Deploying active AirCore, which are also very light-weighted sampling devices, on UAS makes it possible to sample plumes such as for example stack or ship plumes in three dimensions and to probe parts of the atmosphere that are inaccessible otherwise. While industrial installations have already been probed with active AirCore, we newly demonstrated the potential of the technique for probing volcanic emissions studying the degassing plumes of Mt. Etna on Sicily in July 2024. Volcanic plumes are a difficult to assess environment which pose considerable challenges due to high levels of acidity and high particle loads. High-precision in situ measurements are difficult to perform under these conditions and air sampling with active AirCore opens new possibilities to study such plumes as state of the art equipment for high-quality measurements can be applied in the post-flight analysis of the air sample. To compensate for a non-uniform filling of the AirCore sample coil, a new method to map the post-flight analysis data onto the flight track was developed.

Focusing on the redox pair CO and CO_2 which allows conclusions on conditions inside the active crater, we demonstrated how active AirCore in combination with post-flight CRDS measurements of CO, CO_2 and CH_4 can be used to obtain high-precision trace gas data from volcanic plumes. It was found that in the volcanic plumes characterised by elevated CO_2 mole fractions also CO was frequently elevated with the $\Delta CO/\Delta CO_2$ ratio varying over two orders of magnitude. To determine

https://doi.org/10.5194/egusphere-2026-1865
Preprint. Discussion started: 21 May 2026

the mole fraction enhancements, attention has to be paid to the definition of the local background mole fractions which are also strongly influenced by volcanic emissions. Thus, is is important to spend a sufficient amount of flight time in the local background but well away from the plumes.

In the field and during data analysis some weaknesses of the setup and further challenges were identified:

(i) Because the plumes are not easily visible, it is difficult for the UAS pilot to keep the drone inside the plume. For real-time assessment of plume location and extension NDIR CO_2 and electrochemical SO_2 sensor were used. This proved essential to adjust the UAS flight pattern. However, sensor may adversely respond to rapid motion and abrupt changes of directions which should therefore be avoided. To improve sensor data quality and reliability, it needs to be ensured that a sufficiently strong pump is installed for a continuously high air flow over the sensors.

(ii) At Mt. Etna, it was not possible to perform the post-flight analysis of the AirCore samples at the launch site of the UAS. In the mountainous environment, the pressure differences because of the unavoidable altitude changes resulted in a contamination of the samples. Changes of altitude or more generally of ambient pressure should thus be kept at a minimum. It should also be ensured that all tubing connections are leak tight into both direction, i. e. towards over- and underpressures. This may, however, make devices less easy to handle as there are connections that need to be altered frequently and quickly between sampling and analysis mode. As in general for AirCore samples, storage times between sampling and analysis should be kept as short as possible, but it might also be beneficial to keep the time between device preparation and launch short.

(iii) Spiking or depletion of the FG and PG mixtures is necessary to identify the air sample within the analysis time series. Depending on the type of environment to be probed and tracers targeted it is advisable to carefully choose the specific mixture. For the special case shown here, a high-CO gas mixture was found not ideal, because CO contamination related to altitude changes occurred and in addition elevated CO was expected in the volcano plumes.

(iv) The total sampling time is limited by the available UAS power supply and because of the inaccessible terrain flight times were planned conservatively. The spatial resolution of the AirCore sample could be improved with a higher nominal pump flow, which could be obtained using a different critical orifice configuration. These parameters need to be well adjusted to collect as much sample as possible.

(v) Deploying the active AirCore along trajectories with significant pressure gradients results in variable flows. Applying a sampling fraction based retrieval approach, instead of a linear mapping, enables the projection of measurements onto flight tracks even along trajectories characterized by substantial pressure variations. The proposed correction scheme, which accounts for variable flows using a simplified 'inflow–outflow' model, represents a valuable extension, as the results show good agreement with in situ sensor data. This approach eliminates the need to redesign the active AirCore system with a flow-controlled inlet, as previously implemented by Tong et al. (2023), thereby enhancing the overall versatility of the method. Nevertheless, it would be advantageous to activate the remote-controllable pump not until

https://doi.org/10.5194/egusphere-2026-1865
Preprint. Discussion started: 21 May 2026

reaching the plume sampling altitude and to maintain a relatively constant altitude thereafter, in order to minimize the magnitude of the applied corrections.

Some of these aspects may be specific to the deployment of UAS-borne equipment in volcanic plumes. Most applications of the active AirCore technique likely take place in less harsh environments with less extreme conditions for the air sampling equipment.

AirCore samples can be analysed for a range of trace gases for which high-precision and fast continuous flow analysers are available. Also subsampling of the sampled air for subsequent laboratory analysis would be possible, at the expense of spatial resolution and taking into account the limited amount of air available. Overall, the active AirCore technique opens future options for a large number of applications, for example probing further tracer-tracer combinations in volcanic plumes that are of interest for geological studies, but also probing other types of plumes.

https://doi.org/10.5194/egusphere-2026-1865
Preprint. Discussion started: 21 May 2026

Data availability. Observational data from the active AirCore measurements and and the Multi-GAS sensors along the flightpaths are available next to the processed data for volcanic plume evaluation from https://doi.org/10.5281/zenodo.18983895 (Degen et al., 2026).

Author contributions. JD, NB, MB, LB, AE, BG, GG, TH, GO, TJS participated in the field work at Mount Etna. SvH and HC designed and built the active AirCore device, NK contributed to the design and construction of sensor packages and field work preparation. JD, AE and TJS performed post-flight analysis of AirCore samples. JD performed the analysis of the active AirCore data with the help of SvH and TJS, while NB, LB, and BG analyzed the Multi-GAS data. JD and TJS drafted the manuscript, all co-authors contributed to the scientific discussion and improvements of the manuscript.

Competing interests. At least one of the (co-)authors is a member of the editorial board of Atmospheric Measurement Techniques.

Acknowledgements. We acknowledge the contribution of all technical staff who were involved in the instrument development.

Financial support. This work was partially funded by EarthCriSys https://earthcrisys.uni-mainz.de. We would also like to thank the Istituto Nazionale di Geofsica e Vulcanologia, Italy, grant “Progetto INGV Pianeta Dinamico (MUSUNGU)” grant - code CUP D53J19000170001 - funded by the Italian Ministry MIUR (“Fondo Finalizzato al rilancio degli investimenti delle amministrazioni centrali dello Stato e allo sviluppo del Paese”, legge 145/2018).

https://doi.org/10.5194/egusphere-2026-1865
Preprint. Discussion started: 21 May 2026

References

Aiuppa, A., Federico, C., Giudice, G., and Gurrieri, S.: Chemical mapping of a fumarolic field: La Fossa Crater, Vulcano Island (Aeolian Islands, Italy), Geophysical Research Letters, 32, https://doi.org/10.1029/2005gl023207, 2005.

Aiuppa, A., Federico, C., Giudice, G., Gurrieri, S., Liuzzo, M., Shinohara, H., Favara, R., and Valenza, M.: Rates of carbon dioxide plume degassing from Mount Etna volcano, Journal of Geophysical Research Atmospheres, 111, https://doi.org/10.1029/2006jb004307, 2006.

Aiuppa, A., Moretti, R., Federico, C., Giudice, G., Gurrieri, S., Liuzzo, M., Papale, P., Shinohara, H., and Valenza, M.: Forecasting Etna eruptions by real-time observation of volcanic gas composition, Geology, 35, 1115, https://doi.org/10.1130/G24149A.1, 2007.

Aiuppa, A., Giudice, G., Gurrieri, S., Liuzzo, M., Burton, M., Caltabiano, T., McGonigle, A. J. S., Salerno, G., Shinohara, H., and Valenza, M.: Total volatile flux from Mount Etna, Geophysical Research Letters, 35, https://doi.org/https://doi.org/10.1029/2008GL035871, 2008.

Andersen, T., Scheeren, B., Peters, W., and Chen, H.: A UAV-based active AirCore system for measurements of greenhouse gases, Atmospheric Measurement Techniques, 11, 2683–2699, https://doi.org/10.5194/amt-11-2683-2018, 2018.

Baker, A. K., Rauthe-Schöch, A., Schuck, T. J., Brenninkmeijer, C. A. M., Van Velthoven, P. F. J., Wisher, A., and Oram, D. E.: Investigation of chlorine radical chemistry in the Eyjafjallajökull volcanic plume using observed depletions in non-methane hydrocarbons, Geophysical Research Letters, 38, L13 801, https://doi.org/10.1029/2011gl047571, 2011.

Bonaccorso, A., Carleo, L., Currenti, G., and Sicali, A.: The intense explosive activity of lava fountain sequences from Voragine crater at Etna volcano: new insights through high-precision borehole strain recordings, Frontiers in Earth Science, 13, https://doi.org/10.3389/feart.2025.1606006, 2025.

Burgisser, A. and Scaillet, B.: Redox evolution of a degassing magma rising to the surface, Nature, 445, 194–197, https://doi.org/10.1038/nature05509, 2007.

Burton, M. R., Sawyer, G. M., and Granieri, D.: Deep Carbon Emissions from Volcanoes, Reviews in Mineralogy and Geochemistry, 75, 323–354, https://doi.org/10.2138/rmg.2013.75.11, 2013.

Butz, A., Dinger, A. S., Bobrowski, N., Kostinek, J., Fieber, L., Fischerkeller, C., Giuffrida, G. B., Hase, F., Klappenbach, F., Kuhn, J., Lübcke, P., Tirpitz, L., and Tu, Q.: Remote sensing of volcanic CO_2, HF, HCl, SO_2, and BrO in the downwind plume of Mt. Etna, Atmospheric Measurement Techniques, 10, 1–14, https://doi.org/10.5194/amt-10-1-2017, 2017.

Calvari, S. and Nunnari, G.: Reawakening of Voragine, the Oldest of Etna's Summit Craters: Insights from a Recurrent Episodic Eruptive Behavior, Remote Sensing, 16, 4278, https://doi.org/10.3390/rs16224278, 2024.

Crosson, E.: A cavity ring-down analyzer for measuring atmospheric levels of methane, carbon dioxide, and water vapor, Applied Physics B, 92, 403–408, https://doi.org/10.1007/s00340-008-3135-y, 2008.

de Moor, J. M., Fischer, T. P., Sharp, Z. D., King, P. L., Wilke, M., Botcharnikov, R. E., Cottrell, E., Zelenski, M., Marty, B., Klimm, K., Rivard, C., Ayalew, D., Ramirez, C., and Kelley, K. A.: Sulfur degassing at Erta Ale (Ethiopia) and Masaya (Nicaragua) volcanoes: Implications for degassing processes and oxygen fugacities of basaltic systems, Geochemistry, Geophysics, Geosystems, 14, 4076–4108, https://doi.org/10.1002/ggge.20255, 2013.

Degen, J., Bobrowski, N., Boucher, L., Geil, B. H., van Heuven, S., Karbach, N., Schuck, T., and Engel, A.: Active AirCore trace gas measurements at Mount Etna from the 2024 EarthCriSys campaign, https://doi.org/10.5281/ZENODO.18983895, 2026.

Edmonds, M.: New geochemical insights into volcanic degassing, Philosophical Transactions of the Royal Society A Mathematical Physical and Engineering Sciences, 366, 4559–4579, https://doi.org/10.1098/rsta.2008.0185, 2008.

https://doi.org/10.5194/egusphere-2026-1865
Preprint. Discussion started: 21 May 2026

Fischer, T. P., Arellano, S., Carn, S., Aiuppa, A., Galle, B., Allard, P., Lopez, T., Shinohara, H., Kelly, P., Werner, C., Cardellini, C., and Chiodini, G.: The emissions of CO2 and other volatiles from the world's subaerial volcanoes, Scientific Reports, 9, https://doi.org/10.1038/s41598-019-54682-1, 2019.

Foley, S. F. and Fischer, T. P.: An essential role for continental rifts and lithosphere in the deep carbon cycle, Nature Geoscience, 10, 897–902, https://doi.org/10.1038/s41561-017-0002-7, 2017.

Friedlingstein, P., O'Sullivan, M., Jones, M. W., Andrew, R. M., Hauck, J., Landschützer, P., Le Quéré, C., Li, H., Luijkx, I. T., Olsen, A., Peters, G. P., Peters, W., Pongratz, J., Schwingshackl, C., Sitch, S., Canadell, J. G., Ciais, P., Jackson, R. B., Alin, S. R., Arneth, A., Arora, V., Bates, N. R., Becker, M., Bellouin, N., Berghoff, C. F., Bittig, H. C., Bopp, L., Cadule, P., Campbell, K., Chamberlain, M. A., Chandra, N., Chevallier, F., Chini, L. P., Colligan, T., Decayeux, J., Djeutchouang, L. M., Dou, X., Duran Rojas, C., Enyo, K., Evans, W., Fay, A. R., Feely, R. A., Ford, D. J., Foster, A., Gasser, T., Gehlen, M., Gkritzalis, T., Grassi, G., Gregor, L., Gruber, N., Gürses, O., Harris, I., Hefner, M., Heinke, J., Hurtt, G. C., Iida, Y., Ilyina, T., Jacobson, A. R., Jain, A. K., Jarníková, T., Jersild, A., Jiang, F., Jin, Z., Kato, E., Keeling, R. F., Klein Goldewijk, K., Knauer, J., Korsbakken, J. I., Lan, X., Lauvset, S. K., Lefèvre, N., Liu, Z., Liu, J., Ma, L., Maksyutov, S., Marland, G., Mayot, N., McGuire, P. C., Metzl, N., Monacci, N. M., Morgan, E. J., Nakaoka, S.-I., Neill, C., Niwa, Y., Nützel, T., Olivier, L., Ono, T., Palmer, P. I., Pierrot, D., Qin, Z., Resplandy, L., Roobaert, A., Rosan, T. M., Rödenbeck, C., Schwinger, J., Smallman, T. L., Smith, S. M., Sospedra-Alfonso, R., Steinhoff, T., Sun, Q., Sutton, A. J., Séférian, R., Takao, S., Tatebe, H., Tian, H., Tilbrook, B., Torres, O., Tourigny, E., Tsujino, H., Tubiello, F., van der Werf, G., Wanninkhof, R., Wang, X., Yang, D., Yang, X., Yu, Z., Yuan, W., Yue, X., Zaehle, S., Zeng, N., and Zeng, J.: Global Carbon Budget 2024, Earth System Science Data, 17, 965–1039, https://doi.org/10.5194/essd-17-965-2025, 2025.

Giggenbach, W. F.: Chemical Composition of Volcanic Gases, Springer, https://doi.org/10.1007/978-3-642-80087-0_7, 1996.

Goff, F., Love, S. P., Warren, R. G., Counce, D., Obenholzner, J., Siebe, C., and Schmidt, S. C.: Passive infrared remote sensing evidence for large, intermittent CO2 emissions at Popocatépetl volcano, Mexico, Chemical Geology, 177, 133–156, https://doi.org/10.1016/S0009-2541(00)00387-9, 2001.

Heue, K.-P., Brenninkmeijer, C. A. M., Baker, A. K., Rauthe-Schöch, A., Walter, D., Wagner, T., Hörmann, C., Sihler, H., Dix, B., Frieß, U., Platt, U., Martinsson, B. G., van Velthoven, P. F. J., Zahn, A., and Ebinghaus, R.: SO_2 and BrO observation in the plume of the EyjafjallajÃ¶kull volcano 2010: CARIBIC and GOME-2 retrievals, Atmospheric Chemistry and Physics, 11, 2973–2989, https://doi.org/10.5194/acp-11-2973-2011, 2011.

ICOS Research Infrastructure, Apadula, F., Arnold, S., Arriga, N., Bergamaschi, P., Biermann, T., Blandin, E., Blessing, C., Bracci, A., Busetto, M., Bán, S., Bäni, L., Calzolari, F., Chen, H., Colomb, A., Conen, F., Conil, S., Couret, C., Cristofanelli, P., De Mazière, M., Delmotte, M., Di Iorio, T., Elsasser, M., Emmenegger, L., Forster, G., Fratticioli, C., Friedli, J., Frumau, A., Fuente-Lastra, M., Gest, L., Grossmann, J., Hanuš, V., Harris, E., Haszpra, L., Hatakka, J., Heliasz, M., Helle, J., Heltai, D., Hensen, A., Hermans, C., Hermansen, O., Hoheisel, A., Kazan, V., Keronen, P., Kneuer, T., Kolari, P., Komínková, K., Kubistin, D., Kumps, N., Laitinen, A., Langrene, L., Lanza, A., Larmanou, E., Laurent, O., Laurila, T., Legendre, V., Lehner, I., Lehtinen, K., Leskinen, A., Leuenberger, M., Levula, J., Lindauer, M., Lopez, D., Lopez, M., Myhre, C. L., Lunder, C., Mammarella, I., Manca, G., Mandrick, Z., Manning, A., Marek, M. V., Marklund, P., Meinhardt, F., Metzger, J.-M., Miettinen, P., Molder, M., Molnár, M., Montaguti, S., Mölder, M., Müller-Williams, J., O'Doherty, S., Ottosson-Löfvenius, M., Piacentino, S., Pichon, J.-M., Pitt, J., Platt, S. M., Plaß-Dülmer, C., Ramonet, M., Rigouleau, L.-J., Rivas-Soriano, P., Roulet, Y.-A., Scheeren, B., Schmidt, M., Schreiber, M., Schumacher, M., Sferlazzo, D., Sha, M. K., Smith, P., Stanley, K., Steger, D., Steinbacher, M., Sørensen, L. L., Taipale, R., Trisolino, P., Vermeulen, A., Vítková, G., Weyrauch, D., Ylisirniö, A., Yver-Kwok, C., Zazzeri, G., Zwerschke, E., Di Sarra, A., Van Den Bulk, P., Álvarez Hernández, A., ICOS Atmosphere Thematic Centre, ICOS

https://doi.org/10.5194/egusphere-2026-1865
Preprint. Discussion started: 21 May 2026

Carbon Portal, ICOS Carbon and Laboratory, ICOS Central Radiocarbon and Laboratory, and ICOS Flask and Calibration: European Obspack compilation of atmospheric carbon dioxide, methane, nitrous oxide and carbon monoxide data from ICOS stations for the period 1972-2025; obspack_466_ICOSFT2025.3_20251003, ICOS Carbon Portal, https://doi.org/10.18160/46st-devk, 2025.

James, M. R., Carr, B., D'Arcy, F., Diefenbach, A., Dietterich, H., Fornaciai, A., Lev, E., Liu, E., Pieri, D., Rodgers, M., Smets, B., Terada, A., Von Aulock, F., Walter, T., Wood, K., and Zorn, E.: Volcanological applications of unoccupied aircraft systems (UAS): Developments, strategies, and future challenges, Volcanica, 3, 67–114, https://doi.org/10.30909/vol.03.01.67114, 2020.

Karbach, N., Bobrowski, N., and Hoffmann, T.: Observing volcanoes with drones: studies of volcanic plume chemistry with ultralight sensor systems, Scientific Reports, 12, 17 890, https://doi.org/10.1038/s41598-022-21935-5, 2022.

Karion, A., Sweeney, C., Tans, P., and Newberger, T.: AirCore: an innovative atmospheric sampling system, Journal of Atmospheric and Oceanic Technology, 27, 1839–1853, https://doi.org/10.1175/2010jtecha1448.1, 2010.

Karion, A., Sweeney, C., Wolter, S., Newberger, T., Chen, H., Andrews, A., Kofler, J., Neff, D., and Tans, P.: Long-term greenhouse gas measurements from aircraft, Atmospheric Measurement Techniques, 6, 511–526, https://doi.org/10.5194/amt-6-511-2013, 2013.

Kazahaya, R., Varnam, M., Esse, B., Burton, M., Shinohara, H., and Ibarra, M.: Behaviors of Redox-Sensitive Components in the Volcanic Plume at Masaya Volcano, Nicaragua: H2 Oxidation and CO Preservation in Air, Frontiers in Earth Science, 10, https://doi.org/10.3389/feart.2022.867562, publisher: Frontiers, 2022.

Kuhn, J., Bobrowski, N., and Platt, U.: The Interface Between Magma and Earth's Atmosphere, Geochemistry, Geophysics, Geosystems, 23, e2022GC010 671, https://doi.org/https://doi.org/10.1029/2022GC010671, 2022.

La Spina, A., Burton, M., and Salerno, G. G.: Unravelling the processes controlling gas emissions from the central and northeast craters of Mt. Etna, Journal of Volcanology and Geothermal Research, 198, 368–376, https://doi.org/10.1016/j.jvolgeores.2010.09.018, 2010.

Laube, J. C., Schuck, T. J., Baartman, S., Chen, H., Geldenhuys, M., van Heuven, S., Keber, T., Popa, M. E., Tuffnell, E., Voet, F., Vogel, B., Wagenhäuser, T., Zanchetta, A., and Engel, A.: Vertical distribution of halogenated trace gases in the summer Arctic stratosphere based on two independent air sampling methods, Atmospheric Measurement Techniques, 18, 4087–4102, https://doi.org/10.5194/amt-18-4087-2025, 2025.

Liu, E. J., Wood, K., Mason, E., Edmonds, M., Aiuppa, A., Giudice, G., Bitetto, M., Francofonte, V., Burrow, S., Richardson, T., Watson, M., Pering, T. D., Wilkes, T. C., McGonigle, A. J. S., Velasquez, G., Melgarejo, C., and Bucarey, C.: Dynamics of Outgassing and Plume Transport Revealed by Proximal Unmanned Aerial System (UAS) Measurements at Volcán Villarrica, Chile, Geochemistry, Geophysics, Geosystems, 20, 730–750, https://doi.org/https://doi.org/10.1029/2018GC007692, 2019.

Martinsson, B. G., Brenninkmeijer, C. A. M., Carn, S. A., Hermann, M., Heue, K., Van Velthoven, P. F. J., and Zahn, A.: Influence of the 2008 Kasatochi volcanic eruption on sulfurous and carbonaceous aerosol constituents in the lower stratosphere, Geophysical Research Letters, 36, https://doi.org/10.1029/2009gl038735, 2009.

Martinsson, B. G., Friberg, J., Sandvik, O. S., Hermann, M., van Velthoven, P. F. J., and Zahn, A.: Particulate sulfur in the upper troposphere and lowermost stratosphere – sources and climate forcing, Atmospheric Chemistry and Physics, 17, 10 937–10 953, https://doi.org/10.5194/acp-17-10937-2017, 2017.

Membrive, O., Crevoisier, C., Sweeney, C., Danis, F., Hertzog, A., Engel, A., Bönisch, H., and Picon, L.: AirCore-HR: a high-resolution column sampling to enhance the vertical description of CH_4 and CO_2, Atmospheric Measurement Techniques, 10, 2163–2181, https://doi.org/10.5194/amt-10-2163-2017, 2017.

Moretti, R. and Stefánsson, A.: Volcanic and geothermal redox engines, Elements, 16, 179–184, https://doi.org/10.2138/gselements.16.3.179, 2020.

https://doi.org/10.5194/egusphere-2026-1865
Preprint. Discussion started: 21 May 2026

Moussallam, Y., Oppenheimer, C., and Scaillet, B.: On the relationship between oxidation state and temperature of volcanic gas emissions, Earth and Planetary Science Letters, 520, 260–267, https://doi.org/https://doi.org/10.1016/j.epsl.2019.05.036, 2019.

Oppenheimer, C. and McGonigle, A. J. S.: Exploiting ground-based optical sensing technologies for volcanic gas surveillance, Annals of Geophysics, 47, https://doi.org/10.4401/ag-3353, 2009.

Oppenheimer, C., Kyle, P., Eisele, F., Crawford, J., Huey, G., Tanner, D., Kim, S., Mauldin, L., Blake, D., Beyersdorf, A., Buhr, M., and Davis, D.: Atmospheric chemistry of an Antarctic volcanic plume, Journal of Geophysical Research Atmospheres, 115, https://doi.org/10.1029/2009jd011910, 2010.

Oppenheimer, C., Scaillet, B., Woods, A., Sutton, A. J., Elias, T., and Moussallam, Y.: Influence of eruptive style on volcanic gas emission chemistry and temperature, Nature Geoscience, 11, 678–681, https://doi.org/10.1038/s41561-018-0194-5, 2018.

Pering, T., Tamburello, G., McGonigle, A., Aiuppa, A., Cannata, A., Giudice, G., and Patanè, D.: High time resolution fluctuations in volcanic carbon dioxide degassing from Mount Etna, Journal of Volcanology and Geothermal Research, 270, 115–121, https://doi.org/https://doi.org/10.1016/j.jvolgeores.2013.11.014, 2014.

Plank, T. and Manning, C. E.: Subducting carbon, Nature, 574, 343–352, https://doi.org/10.1038/s41586-019-1643-z, 2019.

Platt, U., Bobrowski, N., and Butz, A.: Ground-Based remote sensing and imaging of volcanic gases and quantitative determination of Multi-Species emission fluxes, Geosciences, 8, 44, https://doi.org/10.3390/geosciences8020044, 2018.

Rauthe-Schöch, A., Weigelt, A., Hermann, M., Martinsson, B. G., Baker, A. K., Heue, K.-P., Brenninkmeijer, C. A. M., Zahn, A., Scharffe, D., Eckhardt, S., Stohl, A., and van Velthoven, P. F. J.: CARIBIC aircraft measurements of EyjafjallajÃ¶kull volcanic clouds in April/May 2010, Atmospheric Chemistry and Physics, 12, 879–902, https://doi.org/10.5194/acp-12-879-2012, 2012.

Roberts, T., Dayma, G., and Oppenheimer, C.: Reaction rates Control High-Temperature chemistry of volcanic gases in air, Frontiers in Earth Science, 7, https://doi.org/10.3389/feart.2019.00154, 2019.

Roberts, T. J., Martin, R. S., and Jourdain, L.: Reactive bromine chemistry in Mount Etna's volcanic plume: the influence of total Br, high-temperature processing, aerosol loading and plume–air mixing, Atmospheric Chemistry and Physics, 14, 11 201–11 219, https://doi.org/10.5194/acp-14-11201-2014, 2014.

Rose, W. I., Millard, G. A., Mather, T. A., Hunton, D. E., Anderson, B., Oppenheimer, C., Thornton, B. F., Gerlach, T. M., Viggiano, A. A., Kondo, Y., Miller, T. M., and Ballenthin, J. O.: Atmospheric chemistry of a 33–34 hour old volcanic cloud from Hekla Volcano (Iceland): Insights from direct sampling and the application of chemical box modeling, Journal of Geophysical Research Atmospheres, 111, https://doi.org/10.1029/2005jd006872, 2006.

Salas-Navarro, J., Stix, J., and de Moor, J. M.: A new Multi-GAS system for continuous monitoring of CO2/ CH4 ratios at active volcanoes, Journal of Volcanology and Geothermal Research, 426, 107 533, https://doi.org/https://doi.org/10.1016/j.jvolgeores.2022.107533, 2022.

Sawyer, G. M., Carn, S. A., Tsanev, V. I., Oppenheimer, C., and Burton, M.: Investigation into magma degassing at Nyiragongo volcano, Democratic Republic of the Congo, Geochemistry Geophysics Geosystems, 9, https://doi.org/10.1029/2007gc001829, 2008.

Shinohara, H.: A new technique to estimate volcanic gas composition: plume measurements with a portable multi-sensor system, Journal of Volcanology and Geothermal Research, 143, 319–333, https://doi.org/10.1016/j.jvolgeores.2004.12.004, 2005.

Shinohara, H., Aiuppa, A., Giudice, G., Gurrieri, S., and Liuzzo, M.: Variation of H2O/CO2 and CO2/SO2 ratios of volcanic gases discharged by continuous degassing of Mount Etna volcano, Italy, Journal of Geophysical Research Atmospheres, 113, https://doi.org/10.1029/2007jb005185, 2008.

Symonds, R. B., Rose, W. I., Bluth, G. J., and Gerlach, T. M.: Volcanic-gas studies: Methods, results, and applications, Digital Commons - Michigan Tech (Michigan Technological University), 30, 1–66, https://digitalcommons.mtu.edu/geo-fp/97, 1994.

https://doi.org/10.5194/egusphere-2026-1865
Preprint. Discussion started: 21 May 2026

Tans, P.: Fill dynamics and sample mixing in the AirCore, Atmospheric Measurement Techniques, 15, 1903–1916, https://doi.org/10.5194/amt-15-1903-2022, 2022.

Tans, P. P.: System and method for providing vertical profile measurements of atmospheric gases, US patent number 759701, 2009.

Timmreck, C.: Modeling the climatic effects of large explosive volcanic eruptions, Wiley Interdisciplinary Reviews Climate Change, 3, 545–564, https://doi.org/10.1002/wcc.192, 2012.

Tong, X., van Heuven, S., Scheeren, B., Kers, B., Hutjes, R., and Chen, H.: Aircraft-Based AirCore Sampling for Estimates of N2O and CH4 Emissions, Environmental Science & Technology, 57, 15 571–15 579, https://doi.org/10.1021/acs.est.3c04932, publisher: American Chemical Society, 2023.

Voigt, C., Jessberger, P., Jurkat, T., Kaufmann, S., Baumann, R., Schlager, H., Bobrowski, N., Giuffrida, G., and Salerno, G.: Evolution of CO2, SO2, HCl, and HNO3 in the volcanic plumes from Etna, Geophysical Research Letters, 41, 2196–2203, https://doi.org/https://doi.org/10.1002/2013GL058974, 2014.

Wagenhäuser, T., Engel, A., and Sitals, R.: Testing the altitude attribution and vertical resolution of AirCore measurements with a new spiking method, Atmospheric Measurement Techniques, 14, 3923–3934, https://doi.org/10.5194/amt-14-3923-2021, 2021.

Westra, I. M., Scheeren, H. A., Stroo, F. T., van Heuven, S. M. A. C., Kers, B. A. M., Peters, W., and Meijer, H. A. J.: First detection of industrial hydrogen emissions using high precision mobile measurements in ambient air, Scientific Reports, 14, 24 147, https://doi.org/10.1038/s41598-024-76373-2, 2024.